



Entangled external and internal controls on submarine fan evolution: an experimental perspective

Ross A. Ferguson¹ | Ian A. Kane¹ | Joris T. Eggenhuisen² | Florian Pohl² | Mike Tilston² | Yvonne T. Spychala² | Rufus L. Brunt¹

¹Department of Earth and Environmental Sciences, University of Manchester, Manchester, UK

²Department of Earth Sciences, Utrecht University, Utrecht, the Netherlands

Correspondence

Ross A. Ferguson, Department of Earth and Environmental Sciences, University of Manchester, Oxford Road, Manchester M13 9PL, UK.

Email: ross.ferguson@manchester.ac.uk

Abstract

Submarine fans are formed by sediment-laden flows shed from continental margins into ocean basins. Their morphology represents the interplay of external controls such as tectonics, climate and sea level with internal processes including channel migration and lobe compensation. However, the nature of this interaction is poorly understood. Physical modelling was used to represent the evolution of a natural-scale submarine fan deposited during an externally forced waxing-to-waning sediment supply cycle. This was achieved by running five successive experimental turbidity currents with incrementally increasing then decreasing sediment supply rates. Deposits built upon the deposits of earlier flows and the distribution of erosion and deposition after each flow was recorded using digital elevation models. Initially, increasing sediment supply rate (waxing phase) led to widening and deepening of the slope channel, with basin-floor deposits compensationally stepping forwards into the basin, favouring topographic lows. When sediment supply rate was decreased (waning phase), the slope-channel filled as the bulk of the deposit abruptly back-stepped due to interaction with depositional topography. Therefore, despite flows in the waxing and waning phases of sediment supply having nominally identical input conditions (i.e. sediment concentration, supply rate, grain size, etc.), depositional relief led to development of markedly different deposits. This demonstrates how external controls can be preserved in the depositional record through the progradation of basin floor deposits but that internal processes such as compensational stacking progressively obscure this signal through time. This evolution serves as an additional potential mechanism to explain commonly observed coarsening and thickening-upwards lobe deposits, with abrupt transition to thin fine-grained deposits. Meanwhile within the slope channel, external forcing was more readily detectable through time, with less internally driven reorganization. This validates many existing conceptual models and outcrop observations that channels are more influenced by external forcing whilst internal processes dominate basin floor lobe deposits in submarine fans.

KEYWORDS

Allogenic, autogenic, experimental modelling, sediment gravity flow, submarine fan architecture

This is an open access article under the terms of the Creative Commons Attribution License, which permits use, distribution and reproduction in any medium, provided the original work is properly cited.

© 2020 The Authors. *The Depositional Record* published by John Wiley & Sons Ltd on behalf of International Association of Sedimentologists.

1 | INTRODUCTION

Submarine fans, the terminal portion of sedimentary source-to-sink systems, are amongst the largest sedimentary accumulations on the planet (Normark, 1970; Posamentier and Kolla, 2003; Talling *et al.*, 2007). Shaped by sediment gravity flows which deliver a range of natural and (more recently) anthropogenic materials to deep-water environments, they provide an invaluable record of Earth's climate and tectonic history, and the dispersal of sediment, organic carbon and pollutants in the deep ocean (Emmel and Curray, 1983; Pirmez and Imran, 2003; Deptuck *et al.*, 2008; Gwiazda *et al.*, 2015; Picot *et al.*, 2016; 2019; Rabouille *et al.*, 2019). Both external and internal processes control the morphodynamic evolution and stratigraphic record of submarine fans

(Figure 1; Beerbower, 1964; Cecil, 2003). External controls refer to those outside the sedimentary system, including sea level, climate and tectonics (Normark *et al.*, 2006; Knudson and Hendy, 2009). These factors are responsible for large-scale variations in the rate, volume and routing of sediment supply to deep-marine systems, and for the total available accommodation space (Maslin *et al.*, 2006; Nelson *et al.*, 2009). Internal controls are self-organisation processes, driven by deposition and erosion. They include channel avulsion, levee growth and compensational stacking (i.e. preferential deposition in topographic lows) of lobes and their constituent building blocks; 'lobe elements' (Figure 1; Pr elat *et al.*, 2009; Wang *et al.*, 2011). Understanding these external and internal controls can aid interpretation of Earth's geological and climate record.

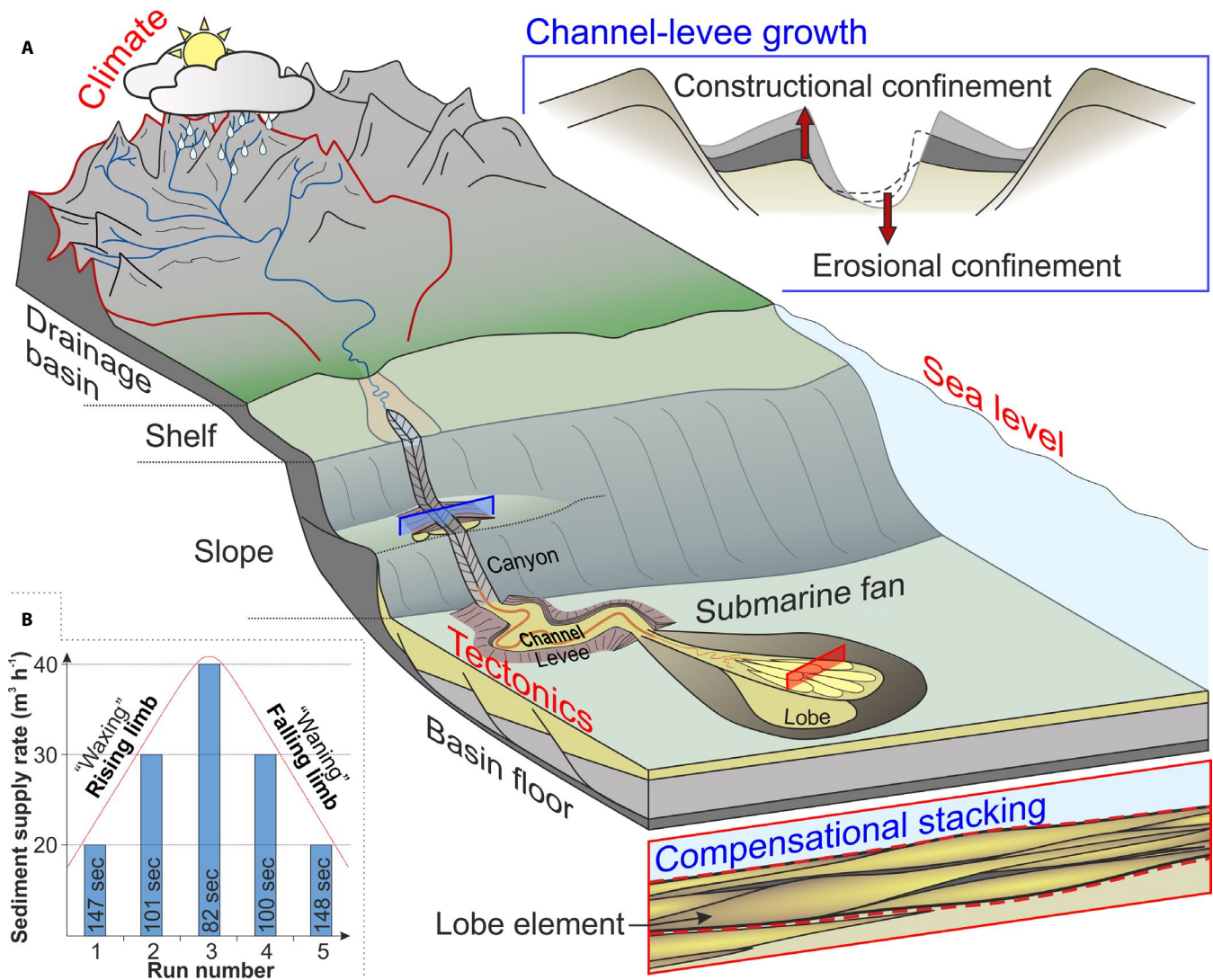


FIGURE 1 Conceptual model of a source-to-sink sedimentary system. (A) External and internal controls (red and blue text respectively) on typical submarine fans. Cross-section locations are indicated on the model. The typical sub-environments of a main channel, levees and lobes are labelled. Compensational stacking image modified from Pr elat *et al.* (2009) and source-to-sink cartoon modified from S omme *et al.* (2009). (B) Variation in sediment supply rate (suspension discharge) between experimental runs. This increase followed by a decrease of sediment supply rate was used to emulate an externally forced waxing-to-waning sediment supply cycle in this study. The duration of each run is indicated on each bar.

Many investigations have been made into the relative control of external and internal forces in fluvio-deltaic environments (Yang *et al.*, 1998; Karamitopoulos *et al.*, 2014; Mikeš *et al.*, 2015; Toby *et al.*, 2019); fewer studies have considered the relative influence of external and internal controls on deep-water sedimentary systems. Source-to-sink analyses have been conducted that variably consider sediment budgeting, routing and provenance to demonstrate the efficiency of sediment delivery to deep water settings (Romans *et al.*, 2009; Sømme *et al.*, 2009; Covault *et al.*, 2010; 2011; Blum *et al.*, 2018). Other studies have investigated the effect of sediment supply and how this directly impacts the architectural evolution of modern submarine channels and lobes (Dorrell *et al.*, 2015; Jobe *et al.*, 2015; 2017). Burgess *et al.* (2019) used power-spectrum analysis to identify a ‘signal bump’ (an increase in the number of spectral peaks at a given frequency) to indicate preserved external signals in stratigraphy.

However, the presence of internal fan organization can make this signal bump difficult to detect (Burgess *et al.*, 2019). This is supported by research that suggests bulk external signals can be modulated or entirely ‘shredded’ by internal processes (Jerolmack and Paola, 2010; Wang *et al.*, 2011; Romans *et al.*, 2016; Harris *et al.*, 2018). In some cases, however, internal processes may amplify external signals creating positive feedback loops, such as increasing channel incision on a slope due to flow confinement within the channel (Hodgson *et al.*, 2016; de Leeuw *et al.*, 2018a). Recent work has shown that external forcing can affect the recurrence of large-volume canyon-flushing turbidity currents, either through sea-level variability (Allin *et al.*, 2018), or tectonically influenced canyon position with respect to its sediment supply system (Jobe *et al.*, 2011). This, and work by Bernhardt *et al.* (2015) on the combined importance of tectonic setting, climate and earthquakes along continental margins further supports the

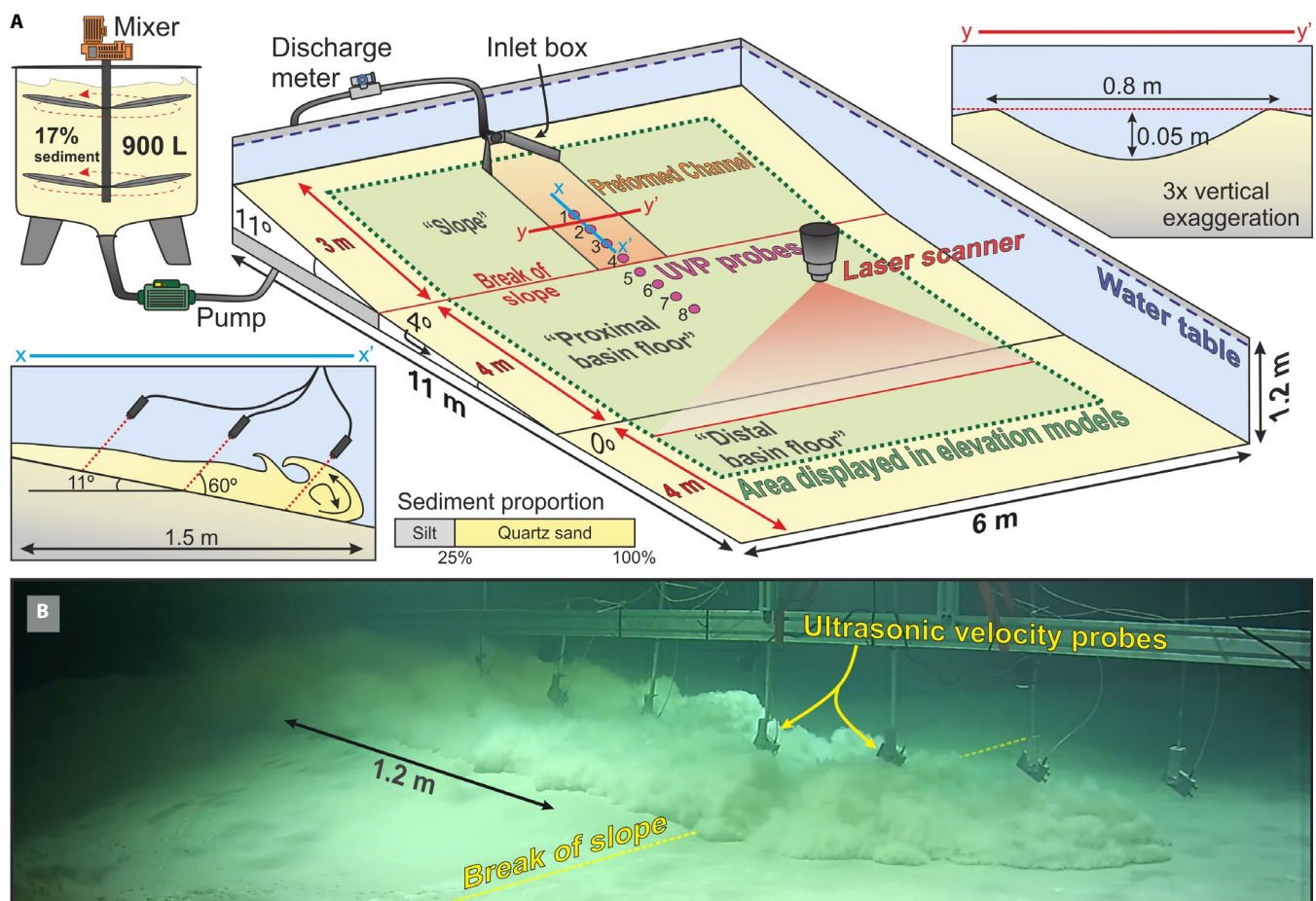


FIGURE 2 3D flume tank set-up at the Eurotank Flume Laboratory. (A) Schematic diagram of the flume tank including key geometries and data collection methods. The sediment–water mixtures were homogenized in a mixing tank before being pumped into the flume tank via the inlet box at the top of the slope. The turbidity currents flowed down a preformed channel on the slope before becoming unconfined at the proximal basin floor. Suspension discharge rates were measured using a discharge meter attached to the supply pipe. Flow velocities were recorded using eight ultrasonic velocity probes (UVPs) positioned along the axis of the channel and across the break of slope at 40 cm intervals. Digital elevation models (DEMs) were generated using a precision laser scanner. The basin was divided into three separate sections based on slope profile: Slope, proximal basin floor and distal basin floor. (B) Image of Run 1 immediately after the head of the flow passed the break of slope. The flow steadily expanded upon reaching the proximal basin floor due to exiting of the confinement.

view that external signals can be expressed in deep-marine environments. As such, to determine the fidelity of fans for tectonic or palaeoclimatic reconstruction, it is essential to understand if and how signals are preserved. If external signals are only partially preserved, it will be necessary to acquire more robust datasets (e.g. multiple core locations) in natural systems in order to confidently reconstruct turbidity current volume and recurrence across sediment routing systems (Jobe *et al.*, 2018).

Here, the question is asked: how is an externally forced sediment supply cycle recorded in the morphology and stratigraphy of a submarine fan? This question was investigated using a series of experimental turbidity currents with incrementally increasing then decreasing sediment supply rates (suspension discharge from a mixing tank) (Figure 1B). Building upon similar experimental studies on submarine channels and lobes (Mohrig and Buttle, 2007; Kane *et al.*, 2008; Cantelli *et al.*, 2011; Janocko *et al.*, 2013a; 2013b;

Fernandez *et al.*, 2014), the morphodynamics of this system are examined together with how the preserved stratigraphic record relates to the external signal. The results are compared explicitly to the exhumed Permian deposits of ‘Fan 3’ in the Karoo Basin, South Africa (Prélat *et al.*, 2009; Groenenberg *et al.*, 2010; Kane *et al.*, 2017). The high stratigraphic resolution in the Karoo Basin allows reasonable comparisons to be made with this study, illustrating the applicability of these results to the interpretation of natural submarine fan deposits.

2 | METHODS

2.1 | Set-up

The experiments were conducted at Utrecht University in the Eurotank Flume Laboratory (Figure 2). The experimental basin was 11 × 6 m in planform and filled to a water level of

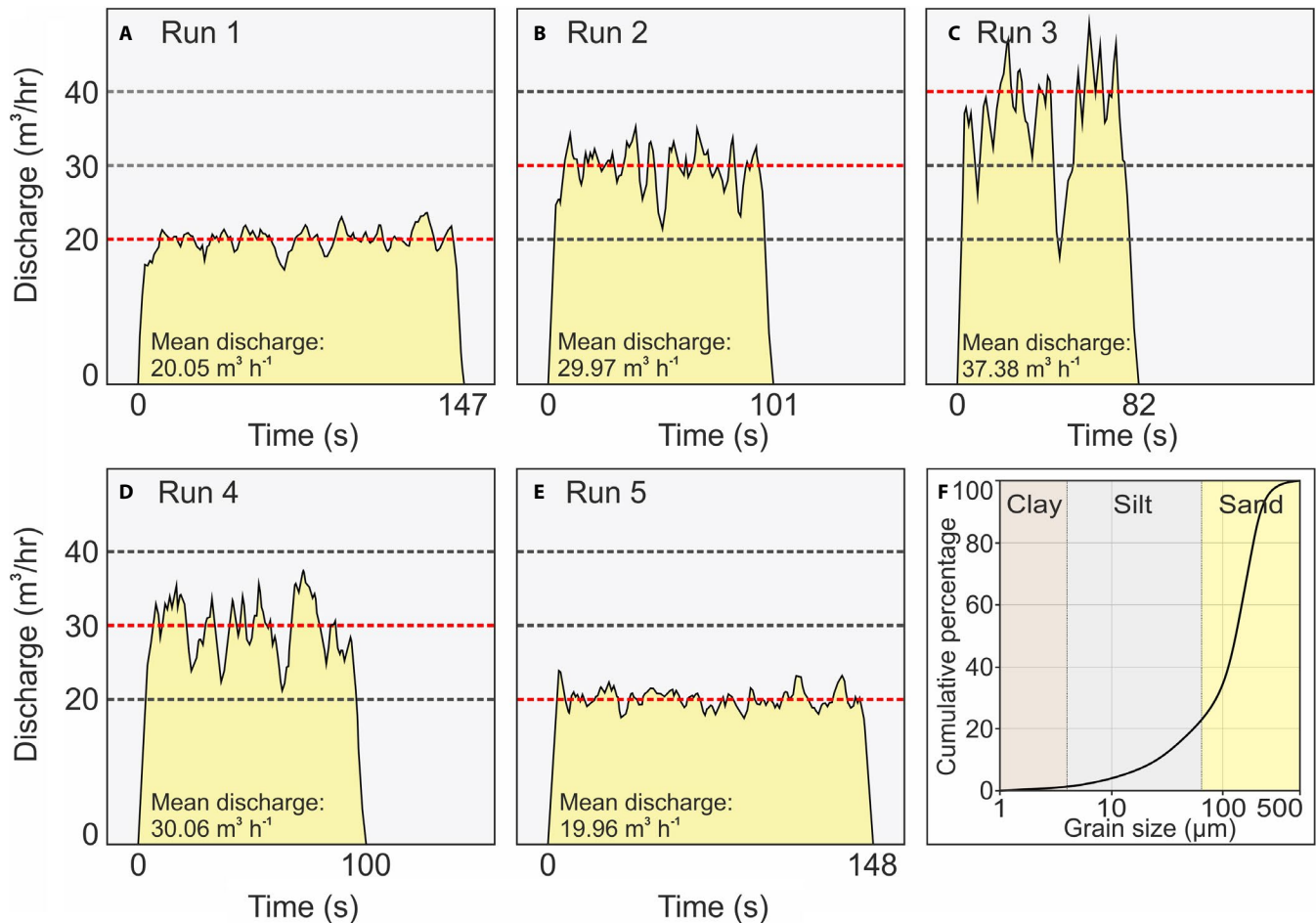


FIGURE 3 Suspension discharge (i.e. sediment supply rate) over time for each run (A–E) and cumulative grain size distribution (F). (A–E) Reference discharge values are given by dashed red lines. When measured sediment supply rate deviated from the reference value (e.g. 20, 30, 40 m³/hr), the pump speed was manually adjusted to compensate. Discharge readings became progressively more difficult to stabilize with increasing discharge rates, resulting in some discharge variability in runs 2, 3 and 4. The mean discharge was calculated using the duration of the whole run minus the first and last 15 s. (F) Cumulative grain size distribution for the suspended sediment in each flow/run and for the erodible substrate of the tank.

TABLE 1 Boundary conditions and flow parameters of the experiments. All categories except ‘discharge/sediment supply rate’ were constant across all five runs.

Suspension volume	900 L
Input sediment concentration	17%
Median grain size	131 μm
Discharge/sediment supply rate (m^3/hr) for runs 1–5, respectively	1. 20 2. 30 3. 40 4. 30 5. 20
Initial channel dimensions (W \times H)	0.8 \times 0.05 m
Slope angle	11°
Slope length	3 m
Proximal basin floor angle	4°
Proximal basin floor length	4 m
Distal basin floor angle	0°
Distal basin floor length	4 m

1.2 m above the horizontal floor. The initial tank bathymetry consisted of an 11° slope of 3 m in length (the “slope”), followed by a 4° slope of 4 m in length (the “proximal basin floor”), ending in a 4 m long horizontal “distal basin floor”. This slope gradient, high for natural settings, promoted flow velocities high enough to erode sediment and bypass sediment to the basin floor (de Leeuw *et al.*, 2016). The tank floor was covered by approximately 20 cm of loose sand of the same grain-size distribution as the turbidity current mixture (Figure 3F) enabling turbidity currents to erode into the substrate. A straight, 0.8 m wide, 0.05 m deep, symmetrical channel form was sculpted into the initial 11° slope from the inlet box to the break of slope (Figure 2A). The dimensions of this initial channel form were selected based on the dimensions of a self-formed channel produced by de Leeuw *et al.* (2016). The turbidity currents entered the basin via an inlet box with an un-erodible base 0.7 m in length and gradually expanding sides before continuing down the sediment covered slope. All boundary conditions were consistent across all runs except for suspension discharge (see Section 2.3 for details; Table 1; Figure 3). Supporting information for this study is provided with the online version of this manuscript.

2.2 | Turbidity current suspension parameters

Prior to each experiment, the sediment mixture was prepared in a separate mixing tank with two impellers that homogenized the mixture (Figure 2). The volume of the suspension (sediment and water mixture) was 900 L in each event; sediment contributed 17% of this. Quartz sand (*Sibelco BR-37*) with

a specific density of 2,650 kg/m^3 constituted 75% (300 kg) of the total sediment suspension volume with the remaining fraction being 100 kg of silt-sized ground glass. The median grain size (D_{50}) of the mixture was 131 μm , with a D_{10} of 25 μm and a D_{90} of 223 μm (Figure 3F). Grain size was analysed using a Malvern Mastersizer particle sizer (Malvern Instruments Limited).

2.3 | Experimental procedure

Five successive sediment-laden turbidity currents entered the basin from the inlet at the top of the slope (Figure 2). These currents were created by pumping the suspension from the mixing tank to the basin via a supply pipe. Suspension discharge (i.e. volume per hour of flow into the tank) was monitored using a discharge meter (Krohne Optiflux 2300) mounted on the supply pipe and regulated using a Labview control system (National Instruments Corporation (UK) Limited). To simulate an external control on the system, in this case a waxing-to-waning sediment supply cycle, the suspension discharge rate was increased between runs 1 to 3 from 20 m^3/hr , to 30 m^3/hr , then 40 m^3/hr , before being decreased back to 30 m^3/hr , and then 20 m^3/hr in runs 4 and 5, respectively (Figures 1B and 3). Discharge rate fluctuated around the reference value in each run, however, this variability averaged out over the course of each run and does not appear to have had a tangible impact on the resultant flows/deposits (Figure 3). Minimum and maximum sediment suspension discharge rates (i.e. boundary conditions) were identified by running a separate series of pilot experiments. A suspension discharge rate of 10 m^3/hr resulted in immediate deposition of the sediment load upon entering the basin whilst 50 m^3/hr resulted in excessive erosion and sediment transport beyond the range of practicable measurement (Figures S1 and S2). Consequently, a minimum suspension discharge rate of 20 m^3/hr and maximum of 40 m^3/hr was used for the main experiment, with 30 m^3/hr used to represent the intermediate phase of the rising and falling limbs (Figure 3). Runs 1–5 ran for 147, 101, 82, 100 and 148 s, respectively (Figure 3), each time draining the 900 L mixing tank. Even though each run was technically an individual ‘flow event’, they are considered to represent protracted phases of sediment delivery to the system. In each phase, a similar volume of sediment was supplied, the effect of the higher discharge being that turbidity currents were larger and more powerful. This scenario should thus be seen as an analogue for increasing then decreasing turbidity current strength during an externally forced cycle (e.g. sea level, climate, or tectonic variability). With this specification in mind, the suspension discharge rate shall henceforth be referred to as ‘sediment supply rate’ for simplicity. A base case equivalent where sediment supply rate was kept constant was not included in this study as earlier works serve to fill this

role and are referred to where appropriate (Fernandez *et al.*, 2014; de Leeuw *et al.*, 2018a; 2018b; Spychala *et al.*, 2019).

Eight Ultrasonic Velocity Profiler (UVP) probes (MET-FLOW, UVP-DUO-MAX, 1 MHz) were positioned 15 cm above the substrate to record the flow field during the experiments. The probes had a spatial resolution of 0.64 mm and a measurement frequency of 1.81 Hz. Their beams were oriented at an angle of 60° relative to the local bed, facing incoming flows along the slope channel axis and across the break of slope at 40 cm intervals (Figure 2). The UVP probes measured the velocity of sediment grains along a vector aligned with the probe axis. Bed-parallel velocity was calculated from the measured data using trigonometry under the assumption that bed-normal velocity was zero. This was plotted against time for each run and was used to infer bed-base deposition

and erosion through time as the bed-base increased or decreased in height (Figures S3 through S7). Time-averaging the velocity data created profiles that enabled analysis of the downslope velocity evolution (Figure 4). These profiles were compared between runs to examine how velocities changed as the experiment progressed. Velocity averages were taken for the entire run durations, minus the head and tail of each flow (first and last 5 s).

Run deposits accumulated sequentially, illustrating how the turbidity currents responded to the evolving topography in the basin. After each experimental run, the basin was drained, and the deposit was scanned using a high-resolution laser scanner. This allowed production of digital elevation models (DEMs) with a horizontal grid spacing of 2×2 mm, and a vertical resolution of <0.5 mm. By comparing DEMs

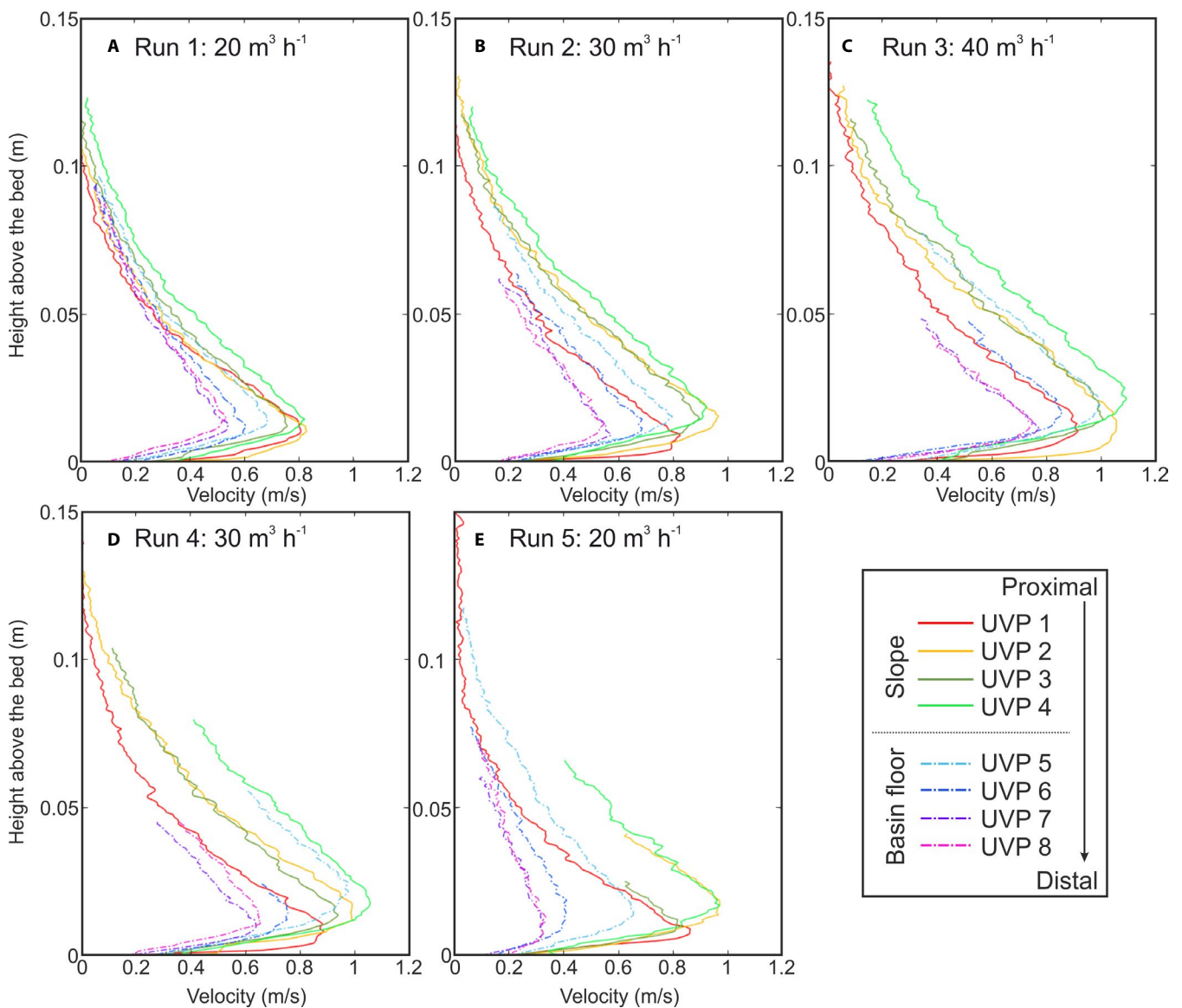


FIGURE 4 Time-averaged velocity profiles for runs 1–5 (A–E). Measurements taken along the centre of the channel and across the break of slope (Figure 2 for location). Solid lines represent ultrasonic velocity probes (UVPs) on the slope and dashed-dotted lines represent UVPs on the basin floor. Velocity averages were taken for entire run durations, minus the head and tail of each flow (first and last 5 s).

from before and after each experimental run, deposition/erosion maps were generated (Figure 5 and Figure S8). Due to high amounts of erosion directly after the inlet box where flows passed over the boundary from un-erodible to erodible substrate, the upper 1 m of the slope channel was restored to its original 0.8×0.05 m geometry to maintain the incoming flow properties between experimental runs.

2.4 | Flow Scaling

To realistically represent a natural system that can erode and transport sediment in suspension downslope, the experimental turbidity currents of this study utilised Shields scaling (Shields, 1936). This approach follows de Leeuw *et al.* (2016) and Pohl *et al.* (2019), using the Shields parameter (τ^*), which is the ratio between bed shear stress and gravitational forces acting on the sediment, and the particle Reynolds number (Re_p), which controls the hydrodynamic condition at the base of the flow (Figure S9). A Shields parameter comparable to natural systems has been achieved in these experiments by using a high sediment concentration (17% of total volume) and a steep (11°) slope (Figure S9; Table S1; Xu *et al.*, 2014; Azpiroz-Zabala, *et al.*, 2017). The particle Reynolds number is subcategorized as ‘hydraulically smooth’ ($Re_p < 5$), ‘transitionally rough’ (Re_p between 5 and 70) or ‘hydraulically rough’ ($Re_p > 70$). Measurements from natural turbidity currents document a transitionally rough regime whilst this experiment plots within the transitionally rough regime in the slope channel, and spans the transitionally rough to hydraulically smooth regimes on the basin floor (Figure S9; Table S1; Xu *et al.*, 2014; Azpiroz-Zabala, *et al.*, 2017). The fine-grained sand used for the flow and substrate ($D_{50} = 131$) ensures transitionally rough flow in the slope channel, promoting erosion through turbulent interaction with the bed.

The Shields parameter and the particle Reynolds number are calculated with:

$$\tau^* = \frac{U^{*2}}{(\rho_s/\rho_f - 1)gD_{50}} \quad (1)$$

$$Re_p = \frac{U^*D_{50}}{\nu} \quad (2)$$

where ρ_s is the sediment density ($2,650 \text{ kg/m}^3$), ρ_f is the current density, g is the gravitational acceleration (9.81 m/s^2), D_{50} is the median grain size ($131 \text{ }\mu\text{m}$), ν is the kinematic viscosity of fresh water at 20°C (1×10^{-6}) and U^* is the shear velocity, estimated using (Middleton and Southard, 1984; van Rijn, 1993):

$$U^* = U_{\max}k \left[\ln \left(\frac{h_{\max}}{0.1D_{90}} \right) \right]^{-1} \quad (3)$$

where U_{\max} is the time-averaged velocity maximum, h_{\max} is the height of the velocity maximum, k is the von Kármán's constant (0.40), and the D_{90} of the grain size is $223 \text{ }\mu\text{m}$. See Table S1 for breakdown of dynamic and sedimentary experimental flow properties.

With this scaling approach the mobility of particles in the flow is ensured, generating turbidity currents that can erode, suspend or deposit sediment. The depositional pattern formed by these flows allows identification of the general response of the system to external and internal controls. Section 4.2 places the experimental deposits into a hierarchical framework to assist comparison with natural settings. However, it should be noted that the purpose of these experiments is not to directly replicate the exact depositional architecture and hierarchy of natural settings, but to provide a practical reference for their development.

3 | RESULTS

3.1 | Fan evolution

The five turbidity currents released into the basin travelled down the slope channel and continued to the unconfined basin floor, creating an evolving pattern of erosion and deposition. The ‘submarine fan’ of this experimental study consists of all areas of the slope and basin floor where erosion and deposition took place and is considered equivalent to both the channel-levee and lobe environments of natural-scale systems (Figure 1). Figure 5 visually documents the morphological evolution of the system using composite erosion/deposition maps and associated cross-sections through the stratigraphy (for individual run erosion/deposition maps see Figure S8). The composite deposit grew with each event, whilst the amount of channel incision and levee deposition varied from run to run (Figure 5 and Figure S8). The results from each run are detailed as follows:

- I The initial topography consisted of a preformed $0.8 \text{ m} \times 0.05 \text{ m}$ channel that extended down the 11° slope before terminating upon the flat, gently dipping (4° then 0°) basin floor.
- II Experimental run 1 ($20 \text{ m}^3/\text{hr}$) transferred most of its sediment load to the basin floor, however, some deposition occurred along the length of the channel (Figure 5). An elongate area was eroded on the right side of the channel axis (looking downstream), widening and deepening the channel. Overbank deposition took place on the flanks of the slope-channel where the flow spilled outside its confinement. Maximum overbank deposition took place directly adjacent to the channel and thinned rapidly away from the channel margins. Upon exiting

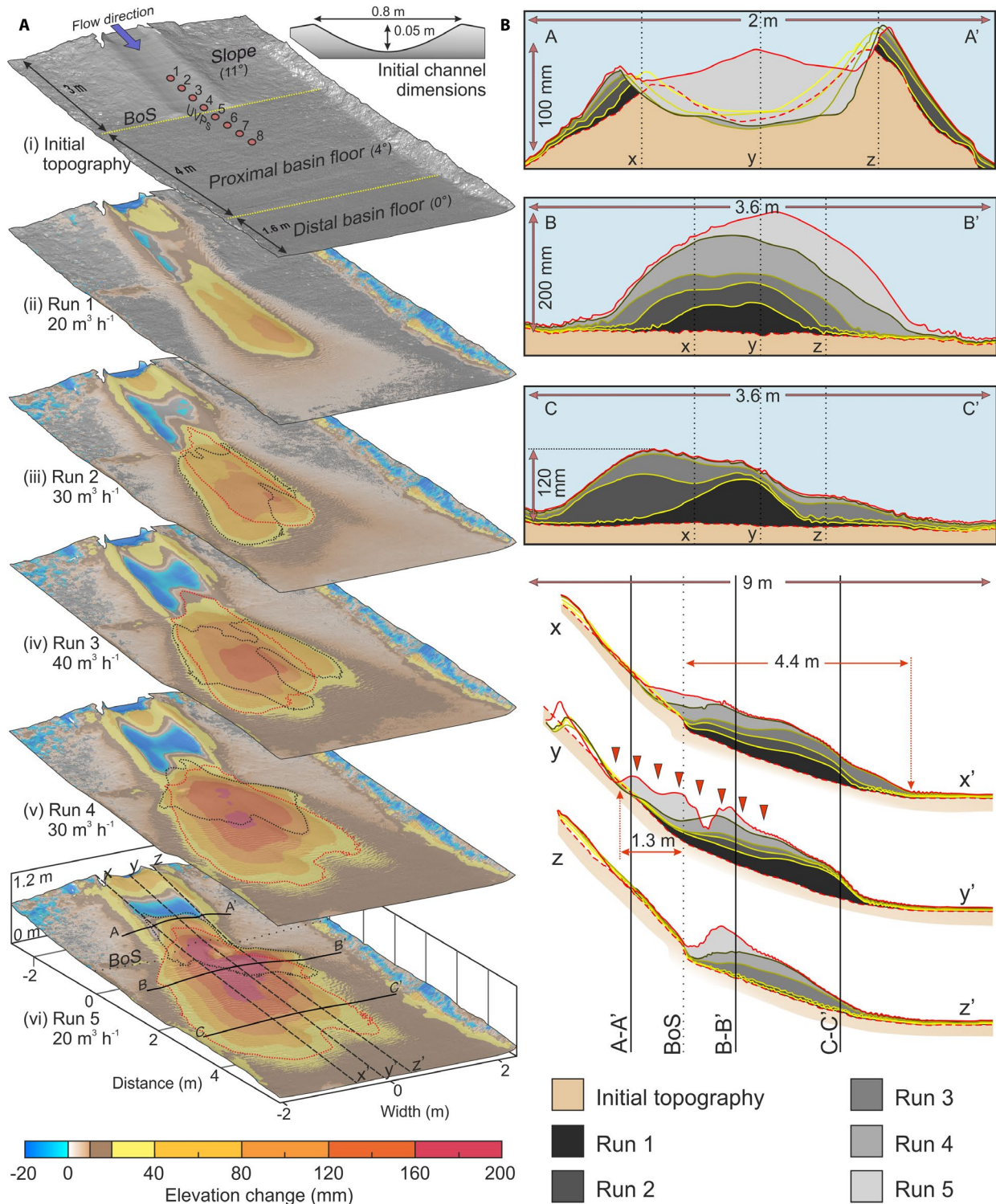


FIGURE 5 Maps of cumulative deposition and erosion and associated cross-sections. (A) Digital elevation models (DEMs) of cumulative deposition (warm colours) and erosion (blue colours) from runs 1 to 5. The dotted red line on each DEM shows the area of the cumulative deposition from the previous runs that is >20 mm thick. The dotted black line shows the area of the deposit from each respective individual run (>20 mm thick). (B) Cross-sections through cumulative deposit (vertical exaggeration $\times 5$). Locations are indicated on run 5 in (A) and intersections are indicated on each cross-section. Red lines denote the final (solid line) and initial (dashed line) topography. Interfaces between runs in each cross-section are gradually darker yellow, from first to last, respectively, to aid differentiation of discrete runs. Red arrowheads on cross-section y-y' indicate UVP probe locations. BoS, break of slope.

the channel confinement at the break of slope, the flow deposited its load centrally on the proximal basin floor in a broadly elongate and lobate shape. The maximum deposit thickness was 107 mm, approximately 2.5 m from the break of slope. A thin (<10 mm) fringe of sediment extended out beyond the main body of the deposit and onto the distal basin floor.

- III During run 2 (30 m³/hr), erosion increased across the slope channel, dominantly towards the right of the channel axis. An increase in overbank deposition was observed, leading to enhanced flow confinement on the slope by both erosional and constructional means. This overbank deposition built upon the deposition from run 1, resulting in wedge-shaped geometries that thinned away from the channel margins; they were consequently classified as levees (Kane *et al.*, 2007; de Leeuw *et al.*, 2018a). On the basin floor, depositional topography created by run 1 deflected the bulk of the flow to the right, causing a lateral shift of maximum deposition (69 mm thick) to the right and compensational stacking of the deposit. A small portion of the flow also deflected to the left of the run 1 deposit, resulting in a thin (*ca* 10 mm) deposit. Overall, the deposit from run 2 extended 12% farther into the basin than the previous deposit (from 3.4 to 3.8 m from the break of slope).
- IV Run 3 (40 m³/hr) represented the peak of the sediment supply curve. Even greater amounts of erosion were observed in the channel axis and substantial overbank deposition occurred. The deposit extended 8% farther into the basin than the deposit of run 2 (to 4.1 m from the break of slope). Compensational stacking continued, with deposition being spread approximately evenly on either side of the initial deposit looking down-flow. Maximum deposit thickness was 53 mm and was found to the left of the basin with respect to flow direction. Notably, this maximum thickness was approximately half that of the deposit of run 1, with sediment being distributed more evenly across the basin floor (see Figure S8 for clarity).
- V Run 4 (30 m³/hr) marked the beginning of waning sediment supply. There was a decrease in channel erosion and limited overbank deposition associated with this reduction in sediment supply rate. On the basin floor, the deposit back-stepped considerably from the position of the run 3 deposit, extending 34% less into the basin than the deposit of run 3 (to 2.7 m from the break of slope). The run 4 deposit exhibited less compensation, stacking more aggradationally (maximum thickness 65 mm) having back-stepped to onlap the slope and begin infilling the slope channel.
- VI Run 5 (20 m³/hr) saw a continuation of the back-stepping trend observed in run 4, extending 41% less into the basin than the deposit of run 4 (1.6 m from the break of slope), with more channel deposition and effectively

no overbank deposition. The maximum deposit thickness was 104 mm, located approximately at the position of the original break of slope (Figure 5A). A small area (*ca* 345 × 445 mm) of erosion developed in the middle of the deposit contemporaneously with the flow event (Figure 5 and Figure S8). This syn-depositional event is evidenced by a lowering of the bed-base recorded in velocity/time plots produced using UVP probe data, indicating that this event took place during the flow event (Figure S7).

3.1.1 | Summary

When sediment supply rate increased, erosion within the channel increased and overbank deposition continued, resulting in a progressive widening and deepening of the channel (Figure 5B, cross-section A–A'). Across the same interval, each successive flow deposit extended farther into the basin than the previous. During this time deposits stacked compensationally (Figure 5). A reversal of the erosional-depositional trend was observed when the sediment supply rate was reduced. Erosion in the channel axis and overbank deposition declined, and the basinal deposit abruptly back-stepped up the slope to fill the channel. The fringe deposits continued to aggrade steadily on the distal basin floor despite forward-stepping, back-stepping and compensation exhibited by the main deposit (Figure 5).

3.2 | Flow-field evolution

A series of UVP probes were placed along the axis of the channel and across the break of slope to record the downslope evolution of the flow field (Figures 2 and 4). Velocities were relatively higher on the slope (0.76–1.09 m/s) (UVPs 1–4), before progressive deceleration took place beyond the break of slope on the basin floor (0.32–0.99 m/s) (Figure 4, UVPs 5–8). This spatial change in velocity was likely driven by the steeper gradient and flow confinement on the slope, versus the gentler unconfined setting of the basin floor. Based on the distribution of erosion and deposition across the experimental basin, it can be inferred that higher velocities on the slope promoted erosion and sediment bypass whilst lower velocities on the basin floor led to deposition.

The spatial evolution of the flow field for runs 1–5 is presented in time-averaged velocity profiles to show how flows developed between runs (Figure 4). The maximum velocity (*U*_{max}) on the slope increased from approximately 0.83 m/s (UVP 2) in run 1, to 1.09 m/s in run 3 (UVP 1) as sediment supply rate was increased between runs. The maximum velocity then decreased in line with the sediment supply rate to

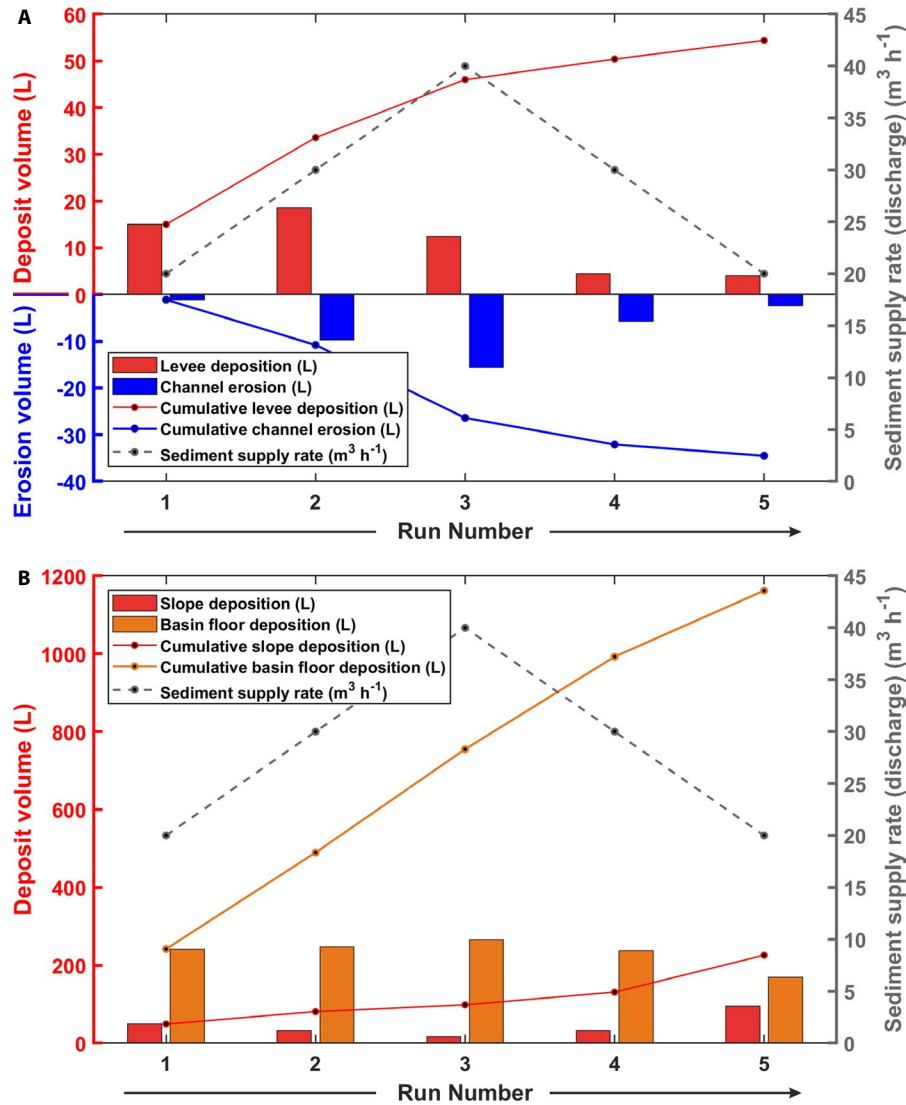


FIGURE 6 Progression of deposition and erosion volume across the five runs. (A) Levee deposition (area of volume calculation outlined in Figure S1) vs. channel erosion. In the waxing phase of sediment supply rate (runs 1–3), the volume deposited by each run was maintained at a relatively high level (>10 L/run). In the waning phase (runs 4 and 5) levee deposition was markedly reduced (<5 L/run). Erosion volume for each run increased and decreased in line with sediment supply rate. The excessive erosion at the inlet box was excluded from the calculation. (B) Slope deposition versus basin floor deposition. Whole slope deposition showed an inverse relationship with sediment supply rate. Most of the slope deposition in runs 1, 4 and 5 occurred within the channel axis. Basin floor deposition decreased by 68 L in run 5. This is associated with a marked increase in slope deposition as the basinal deposit back-stepped onto the slope.

approximately 0.97 m/s in run 5 (UVPs 1 and 2). This trend of increasing then decreasing flow velocity with sediment supply rate was also documented on the basin floor (UVPs 5–8). Uncertainty is attached to the later (e.g. run 5) basin floor readings as the highly variable flow pathways created by the depositional topography (see Figure 5A) hindered the probes' ability to accurately record the dominant flow direction. Despite this uncertainty, the broad trends of increasing velocities with increasing sediment supply rate were consistent across the slope and basin floor (Figure 4). This flow-field evolution correlates with the depositional trend of a forward then back-stepping depositional system, demonstrating a clear link between process and product.

4 | DISCUSSION

4.1 | Expression of external signals and internal processes in submarine fan environments

4.1.1 | External versus internal controls on slope channels

External factors, in this case a waxing-to-waning sediment supply rate, set the initial boundary conditions for submarine fan development. These external drivers (e.g. tectonics, sea level and climate) promote conditions whereby sediment delivery

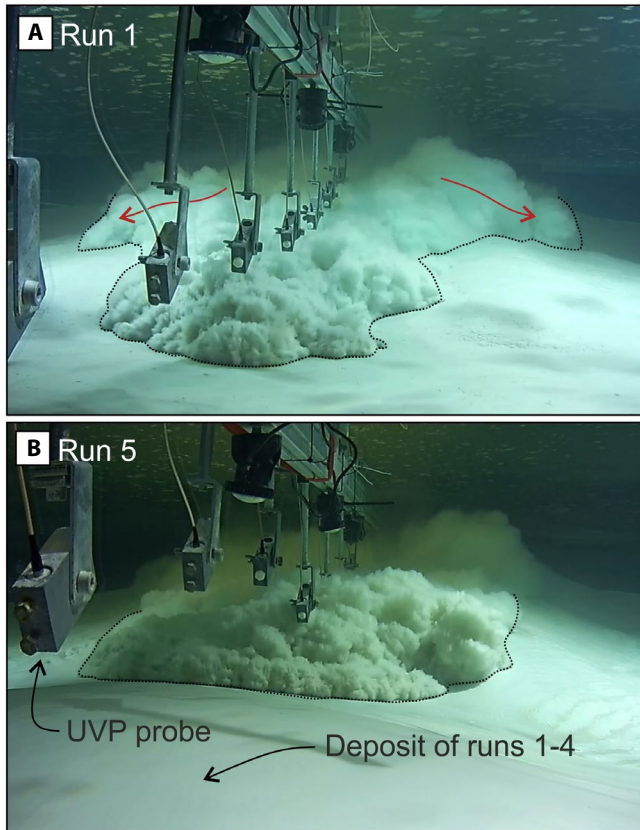


FIGURE 7 Photos of turbidity currents from runs 1 (A) and 5 (B) as they reached the break of slope, just prior to loss of channel confinement. Runs 1 and 5 represented the beginning and end of the waxing-to-waning sediment supply and had the same sediment supply rate ($30 \text{ m}^3/\text{hr}$). Flow direction was towards the camera. The currents are outlined with a dotted black line for clarity. For scale, UVPs are spaced at 40 cm intervals. (A) The current of run 1 overspilled the channel on either side as indicated by the red arrows. (B) The current of run 5 is almost entirely contained within the widened and deepened channel.

may be more (or less) likely and can create or remove accommodation for sediment deposition (King *et al.*, 2009; Clare *et al.*, 2014; Harris *et al.*, 2016; Allin *et al.*, 2018). In this experiment, sediment supply rate was the primary control on the amount of erosion/deposition that occurred within the slope-channel. Low sediment supply rates resulted in relatively high amounts of deposition within the channel and vice-versa (Figure 6). The volume of overbank (levee) deposition in runs 1–3 stayed relatively high ($>10 \text{ L}$ for each run) as sediment supply rate increased, despite the channel being progressively widened and deepened by channel erosion and overbank deposition (Figures 5B and 6; Figure S8). These growing levees would normally be predicted to progressively confine the flows due to the flows becoming smaller with respect to the channel form (Hodgson *et al.*, 2016; Shumaker *et al.*, 2018). Instead, the levees continued to be overtopped; probably due to flows becoming progressively larger, experiencing more

turbulent mixing and decreased grain-size stratification as the sediment supply rate was increased between runs (Rouse, 1939; Kneller and McCaffrey, 1999; de Leeuw *et al.*, 2018a; Eggenhuisen *et al.*, 2019). When sediment supply rate was reduced, overbank deposition lessened ($<5 \text{ L}$ in each run) and deposition in the channel axis increased as the flows of runs 4 and 5 were now substantially underfit with respect to the new evolved channel dimensions (Figures 6 and 7; de Leeuw *et al.*, 2018b). As the incoming flow conditions for runs 1 and 5 were identical, the decrease in overbank deposition in run 5 is likely due to increased erosional and constructional confinement (Figures 5B and 6; Figure S8). This is more in line with the convention whereby channels in disequilibrium work towards an idealized geometry as the experimental flows latterly experienced reduced overbank deposition, predominantly depositing within the channel (Figures 6 and 7; Kneller, 2003; Hodgson *et al.*, 2016; Shumaker *et al.*, 2018). Previous studies have identified similar depositional trends to those observed here in channel-levee outcrops and attributed them to either external variation of flow magnitude, or the internal processes of overbank aggradation and sediment transfer through the channel (Kane and Hodgson, 2011). This study suggests that not only are these scenarios plausible, but also that both processes may act upon the system concurrently. Rather than progressively less sediment being overspilled with each run through the experiment, consistently high amounts of overspill were observed in the waxing phase which abruptly declined in the waning phase (Figure 6). This newly documented evolution is driven by the interplay of sediment supply rate (external) and constructional/erosional channel confinement mechanisms (internal).

Comparable experiments of de Leeuw *et al.* (2018a) demonstrated that submarine channel evolution is a function of both levee growth and channel floor aggradation/degradation, and that fining upwards grain-size trends in levees need not necessarily reflect external forcing. This trend of constructional and erosional confinement has also been documented in various recent and ancient datasets (Deptuck *et al.*, 2007; Janocko *et al.*, 2013b; Hodgson *et al.*, 2016; Kneller *et al.*, 2020). Previous research has shown similar findings in different depositional settings such as alluvial fans and river deltas where overbank flow, cut-through and back-filling of channels play an important role (Hoyal and Sheets, 2009; Hamilton *et al.*, 2013; de Haas *et al.*, 2016). The results reported here agree with these previous studies but also suggest that external forcing can directly influence the rate, timing and distribution of erosion and deposition in submarine channel-levee systems.

The increase in flow confinement within the slope channel documented in runs 1–3 of this study improved the channel's efficiency at bypassing sediment to the basin floor (de Leeuw *et al.*, 2018b), but not to the same extent as the external signal of increasing sediment supply rate. de Leeuw *et al.* (2018b) showed using a similar experimental set-up that a narrower

and deeper channel promotes greater flow thickness and velocity. They documented an increase in flow velocity of *ca* 0.03 m/s when the channel width was dropped from 1.2 to 0.53 m. This is approximately nine times less than the velocity increase documented between runs 1–3 in this study (0.27 m/s at UVP 2), indicating that the external signal of sediment supply rate was the dominant control on the flow field evolution.

It is possible that by altering the pattern of sediment supply to the experimental system from flows with quasi-steady sediment supply rate that incrementally increased between runs, to flows that also had internal sediment supply rate variability (i.e. second order supply cycles) sediment distribution in the basin would be affected. However, physical and numerical experiments by Li *et al.* (2016) and Foreman and Straub (2017) on deltaic and alluvial systems suggest that external controls (they use relative sea level and climate oscillation, respectively) had to be of a greater spatial and temporal scale than that of the internal dynamics of the system. This suggests that smaller-scale variation than that applied to this experimental system may be undetectable in the depositional record, particularly in increasingly distal settings. Supporting this, the recorded discharge rates reported here show varying amounts of deviation from the reference discharge values (sediment supply rate) but there is no evidence of this small-scale variability in the resultant deposits (Figure 3).

4.1.2 | External versus internal controls on basin floor deposition

Meanwhile on the basin floor, an entirely different signature was left by the interaction of external and internal controls. In the waxing phase of sediment supply, increased flow velocities enabled flows to transport sediment progressively farther into the basin (Figure 5; Sychala *et al.*, 2019). If sediment supply rate had not been increased between runs, it is possible that the basin floor deposits would not have forward stepped to the same extent. Using a similar experimental set-up with constant sediment supply rate, Fernandez *et al.* (2014) showed that lobes deposited across a slope break immediately back-step, never extending beyond the initial deposit. In the experiments reported herein, increasing flow confinement on the slope partially increased the flow's ability to transport sediment basinwards (Figure 5B, cross-section A–A'; de Leeuw *et al.*, 2018b), enhancing the external signal of increasing sediment supply rate. This internal slope process was masked in the waning phase of the series (runs 4 and 5) by abrupt back-stepping of the basin floor deposits, comparable to channel back-filling documented by Hoyal and Sheets (2009) in a deltaic experimental setting. During the waning phase, internal depositional relief reduced the local slope gradient to the point where it became horizontal and even adverse

to the main slope gradient. This alteration of the basal topography enhanced the back-stepping trend of the waning phase by reducing flow velocities earlier in the basin and promoting increased slope deposition (Figure 6B). The back-stepping trend features a more pronounced shift in depositional loci than the initial forward-stepping trend (Figure 5 and Figure S8). As such, it is likely that the effect of the depositional relief was strong enough to force back-stepping of the system irrespective of lowering sediment supply rate. This is supported by the observation of immediate back-stepping in Fernandez *et al.*'s (2014) experiments with constant sediment supply. It is therefore insinuated that internal forcing on the basin floor assumed a progressively larger role in deposit distribution relative to external forcing. Regardless of the sediment supply signal, internal organization through lobe compensation, depositional topography and consequent back-stepping pervades as a dominant feature on the basin floor, supporting the observations of previous studies (Cantelli *et al.*, 2011; Fernandez *et al.*, 2014; Burgess *et al.*, 2019).

4.1.3 | Comparison of slope versus basin floor environments

The implication behind the above findings is that the roles of both external and internal forces are contrasting depending on the position along the depositional profile and the temporal stage of the submarine fan's development. These findings are comparable to those of Allin *et al.* (2018) who showed how an external signal propagated by sea-level cycles becomes progressively less clear from proximal to distal in the Nazaré depositional system. Within the slope channel environment of these experiments, an amplification of the external signal by progressive flow confinement was observed, promoting sediment deposition deeper in the basin. Concurrently on the basin floor, internally induced compensational stacking and depositional relief augmented the external signal to the point of forcing abrupt and pronounced back-stepping towards the latter half of the series (Figure 5). Deposits from nominally identical input conditions in the waxing and waning limbs of supply cycles are therefore very different. This is reflected in the recorded velocity profiles which show highly variable time-averaged flow velocities in run 5 compared to run 1, presumably due to the evolved channel dimensions and complex depositional topography (Figure 4).

Compensational stacking and back-stepping through time as seen here has been documented similarly in modern sea floor (Deptuck *et al.*, 2008; Prather *et al.*, 2012; Jobe *et al.*, 2017), experimental (Cantelli *et al.*, 2011; Fernandez *et al.*, 2014) and numerical (Burgess *et al.*, 2019) data sets. The results of this study build upon these previous works, indicating that when external factors (in this case waxing-to-waning

sediment supply rate) are present they have a stronger influence upon channels, whilst basin floor deposition is dominated primarily by internal processes. It is possible that by testing a wider range of boundary conditions (e.g. different grain sizes, channel slope/width/depth) that other styles of external forcing may be represented. This may express the relationship between external and internal controls on submarine slopes and basin floors subtly differently. Fortunately, the effect of different boundary conditions has been evaluated in previous works (de Leeuw *et al.*, 2018b; Sychala *et al.*, 2019). For example, de Leeuw *et al.* (2018b) demonstrated how channels with low width:depth ratios bypass sediment more efficiently to the basin floor than channels with high width:depth ratios. These findings support the broad trends of submarine fan development documented herein, suggesting that examining external forces by varying different boundary conditions may produce largely similar results.

External factors having a stronger impact upon slope channel-levees than basin floor depositional environments have substantial implications. Whilst levees are commonly well-preserved, the channel axis has inherently lower preservation potential than basin floor deposits. The deposits of smaller-scale turbidity currents within the channel are known to be 'flushed' out of the channel system by larger flows, removing stratigraphy (Allin *et al.*, 2018; Jobe *et al.*, 2018). Consequently, there is a high risk that the channel-fill deposits that contain the record of the external signal are not preserved in the rock record. When considering the channel-fill deposits of these experiments for example, only the deposits associated with back-filling are recorded and nothing of the erosive runs 1–3 that came before (Figure 5B; cross-section A–A'). Only by using this high-resolution data set it is possible to identify the complex relationship between the channel axis and levees through time and attribute this to external and internal factors (Section 4.1.1). In natural modern and ancient datasets, extracting explicit information to differentiate between external and internal mechanisms within slope channels will continue to be challenging due to resolution issues. By investigating modern systems with repeat monitoring over short time-scales the degree of preservation within the channel axis may be more confidently resolved. In contrast, basin floor deposits in natural settings do not record smaller turbidity currents that fail to reach them, but their preservation potential is substantially higher than channels due to the predominantly depositional nature of basin floor environments.

These results suggest that whilst slope channel-levees may provide the best record of external signals, they have low preservation potential in the channel axis. Meanwhile basin floor lobes feature a lower resolution record of external signals, but a better-preserved depositional record. Section 4.3 provides a possible mechanism whereby it still may be possible to use this limited rock record in tandem with the observations of this study to interpret stacking patterns in outcrop and core.

4.2 | Hierarchy of basin floor depositional elements

Basin floor lobe deposits have been recognized as hierarchical in nature due to their compensational stacking (Deptuck *et al.*, 2008; Prélat *et al.*, 2009; Straub and Pyles, 2012; Grundvåg *et al.*, 2014; Jobe *et al.*, 2017). To assist comparison between the experimental deposits of this study and those of larger-scale natural submarine fan systems, the lobe deposit hierarchy of Prélat *et al.* (2009) is used (Figure 8). This scheme consists of four components: one or more 'beds' - the product of individual flow events - stack to form a 'lobe element'. Lobe elements are generally a few kilometres in length and width and a few metres thick (Prélat *et al.*, 2010). One or more lobe elements fed from a single channel stack to form a 'lobe'. An updip avulsion or migration of the channel creates a new lobe, stacking on top of the earlier lobe to form a 'lobe complex'. Whilst the individual runs of this study were individual flow events and so were technically beds by the above definition, the key aim was to represent a protracted phase of waxing-to-waning sediment supply to a submarine fan over geological time. This would be very difficult to resolve by considering five flow events in isolation. Each run of this study is consequently considered to represent a lobe element, with the whole series of runs representing a lobe (sensu Sychala *et al.*, 2019). This approach is further supported by evidence that beds stack more aggradationally relative to lobe elements which show more pronounced compensation (Straub and Pyles 2012). Jobe *et al.* (2017) effectively show how bed-scale deposits can still display compensation in modern intra-slope settings, however, the compensation recorded in these experiments is substantially more pronounced than that of the beds recorded in the western Niger Delta slope.

Despite the usefulness of comparing this paper's data to hierarchical schemes of natural systems, doing so highlights some of the difficulty in applying strict organizational structure to nature. In the transition between the channel and lobe in this experiment, the deposition is clustered or 'anti-compensational' across all five runs (Figure 5B, cross-section B–B'), with the deposits stacking on top of each other (Straub *et al.*, 2009). This aggradational character is likely due to the channel position effectively controlling the depositional location. Therefore, it appears that compensation is not able to develop until a certain distance down-dip from the channel-lobe transition (Figure 5B, cross-section C–C', and Figure 8).

If the simplified view is taken that discrete 'hierarchical components' (i.e. bed-sets, lobe elements, lobes and lobe complexes) are internally composed of clustered units, at the break of slope in this study there was only a single hierarchical component. There was no deposit compensation at this location (Figure 5B, cross-section B–B'), implying that multiple lobe elements did not exist there. If this is assumed to be true, the hierarchical component becomes more of a local geometric

definition rather than a hierarchically delineated correlatable unit. This raises fundamental questions about depositional hierarchy and its spatial applicability. For example, how do hierarchical components vary in their geometry from proximal to distal and what are the implications for their practical application? The results reported here suggest that lobe element-scale strata may be more challenging to distinguish near the channel to lobe transition where deposits behave more aggradationally, versus the lobe fringe where compensation is common.

4.3 | Implications for interpretation of submarine fan records

The evolution from forward-stepping and compensational stacking, to abrupt back-stepping recorded in this experimental fan can be used as a possible explanation for bed stacking patterns commonly observed in outcrop and subsurface cores from examples in the rock record. A thickening and coarsening-upwards trend in submarine lobe deposits has been described from several outcrops and this is often followed by an abrupt transition to thin-bedded fine grained

sediments, usually interpreted as hemipelagic abandonment or distal fringe facies (Pickering, 1983; Grecula *et al.*, 2003; Bernhardt *et al.*, 2011; Macdonald *et al.*, 2011). The coarsening and thickening-upwards succession is typically attributed to the local depositional environment becoming progressively higher in energy, transitioning from marginal to more axial fan localities (Kane and Pontén, 2012). However, the forcing mechanism for the abrupt transition from thick sandstones to packages of fine-grained sediments is less clearly understood. It is argued here that the evolution of the ‘experimental lobe’ in this study provides an elegant way to explain this stacking pattern. Figure 9 shows the temporal evolution of the experimental lobe in both 2D and 3D space. The 2D diagram (Figure 9A) displays the forward and back-stepping of the lobe from run 1 to 5, by showing how the location of the maximum deposit volume shifts in a dip-oriented direction through time. The 3D cross-sectional diagram (Figure 9B) emphasizes the internal complexity of the lobe, particularly how lobe element compensation is more pronounced distally. Supporting these images is a series of sedimentary logs from Fan 3 of the Permian Skoorsteenberg Formation, Karoo Basin, South Africa (Figure 9C; Kane *et al.*, 2017). The highlighted

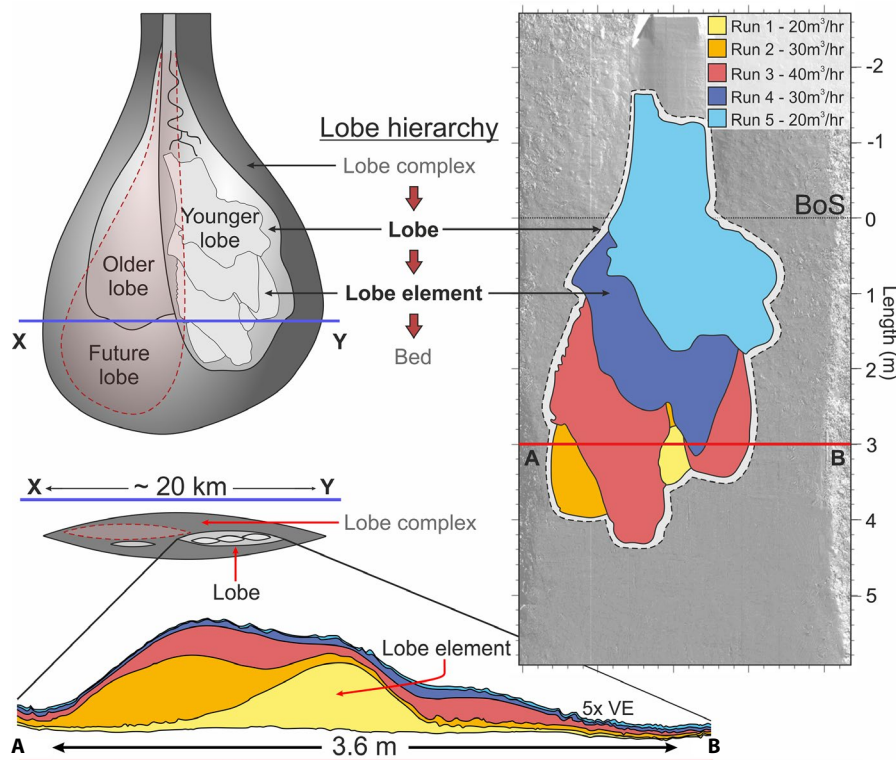


FIGURE 8 Experimental deposits are placed within a hierarchical scheme for lobe deposits (modified from Groenenberg *et al.*, 2010). Whilst the deposits from each run constituted a single flow event and were therefore technically ‘beds’ by the strictest definition, they bore a closer architectural resemblance to ‘lobe elements’ (Prélat *et al.*, 2009), with pronounced compensational stacking (Straub and Pyles, 2012) and classical lobate shape. This has aided comparison to larger-scale natural systems. The plan-view image of the experimental ‘lobe’ displays the main deposit of the lobe elements (>10 mm thick) whilst the corresponding colour-coded cross-section displays the entire lobe thickness, including the thin fringes of later lobe elements deposited in runs 4 and 5. The ‘future lobe’ indicated by the dashed red line on the natural-scale system extends farther into the basin to represent hypothetical progradation of the lobe complex. BoS, break of slope.

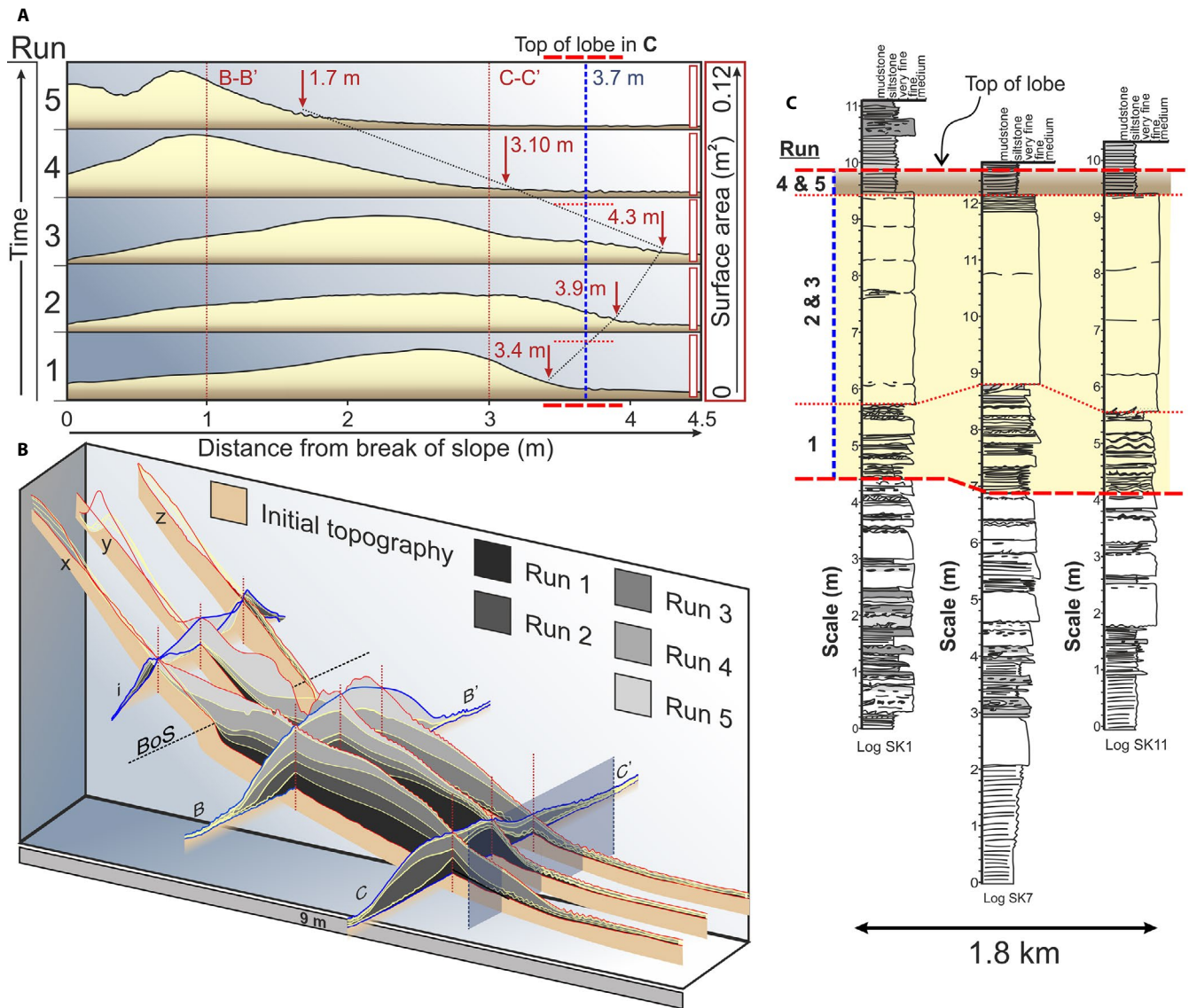


FIGURE 9 Interpreting deposit stacking patterns in nature using experimental observations. (A) Variation in deposit volume with distance from the break of slope for each run. Cross-sectional surface area was used as a proxy for deposit volume by calculating the difference between pre-run and post-run topography with high resolution (every 2 mm) perpendicular to the dominant slope (Spychala *et al.*, 2019). Red arrows indicate the distal end of axial deposits (values taken from DEMs in Figure 5). The dashed blue line and cross-cutting dashed/dotted red lines are representative of the corresponding lines in (C). Cross-section intersections are indicated by vertical dashed red lines. (B) Internal architecture of the cumulative deposit represented in three-dimensional space using composite cross-sections (see Figure 4B). Deposit fore and back-stepping, as well as lateral shifting, can be observed. The semi-transparent blue panel is representative of the dashed blue line in (C). (C) Comparative sedimentary logs from the outcropping ‘Fan 3’ of the Skoorsteenberg Formation, Karoo Basin, South Africa (modified from Kane *et al.*, 2017). The yellow shaded interval highlights older interpretations (Prélat *et al.*, 2009; Kane *et al.*, 2017) of ‘Lobe 5’ whilst this study reinterprets the top of the lobe as within the thin-bedded, fine-grained deposits above this sandstone. The accompanying dashed blue line is depicted in both (A) and (B) (as a semi-transparent blue panel) to indicate the outcrop’s comparative position on the experimental deposit. The abrupt back-stepping in this model could explain the abrupt facies changes commonly observed in outcrop and core at lobe-scale.

zone on these logs indicates ‘Lobe 5’, a typical example of this coarsening and thickening trend that abruptly reverts to siltstone. Conventionally, the siltstone at the top of the sandstone has been interpreted to represent one of two models: (a) A condensed section of hemipelagic deposition during an externally driven reduction in sediment supply (Johnson *et al.*, 2001; Hodgson *et al.*, 2006); (b) Lateral fringes of additional

lobes, representing system-internal lobe-scale compensation (Prélat *et al.*, 2009). Recent studies are beginning to challenge the notion that mud deposition within active submarine fan systems is purely hemipelagic in nature, more likely representing the distal fringe of active systems (Boulesteix *et al.*, 2019). This suggests that it is unlikely that the siltstones above the lobe 5 sandstones are reflecting a complete

'shutdown' of sediment supply. The model of lateral fringe aggradation of later lobes is more likely due to widely recognized compensational stacking and associated grain-size distributions in lobe deposits (Deptuck *et al.*, 2008; Prélat *et al.*, 2009; Straub and Pyles, 2012). However, this does not explain the abruptness at which deposits transition to fine-grained sediments (Figure 9C). Proposed here is an adapted version of this model whereby this transition can be more readily explained by a combination of compensational stacking and rapid back-stepping of 'lobe elements' (Figures 8 and 9). It is suggested that depositional relief and waning sediment supply as observed in these experiments drives this evolution, leading to the stratigraphic patterns observed in nature.

Identification of back-stepping deposits from compensationally lateral-stepping deposits will always be challenging in outcrop and core due to the likelihood of similar facies being present in distal along-axis and off-axis trends. Differentiating criteria for back-stepping deposits would include: (a) abrupt vertical transition from sand-dominated to mud-dominated facies; (b) beds that thin across-strike in both directions, rather than thickening laterally into an adjacent lobe axis; and (c) a preference for deposition of hybrid event beds relative to ripple-laminated deposits. Hybrid event beds have been documented to characterize deposition in frontal fringe environments where back-stepping might be expected, whilst ripple-laminated deposits show preference for the lateral fringe (Spychala *et al.*, 2017). Identifying any or even all of these criteria would not mean unequivocal proof for back-stepping due to additional basinal complexity such as complex regional topography, however, they would provide a basis for assessing submarine fan evolution within a regional context. Identification of abruptly back-stepping strata in the rock record of any given system would have implications for our understanding of the distribution of sediment within that basin. If strata are identified as abruptly back-stepping, this suggests that the system may have built depositional relief to the point of forcing the system backwards irrespective of external sediment supply, perhaps due to a degree of (scale-dependent) basin confinement. If no evidence for abrupt back-stepping is observed, this may imply that incoming flows have had space to continue to stack compensationally until sediment supply has waned, allowing for a more 'classic' gradational upwards transition to fine grained deposits.

Previous workers placed the top of Lobe 5 (Figure 9C) at the top of the thick sandstone unit (Prélat *et al.*, 2009; Kane *et al.*, 2017). However, this study suggests that the top of the lobe (i.e. the end of the sedimentary cycle) at a fixed point within the system is not necessarily where the thickest/coarsest deposits are observed but may lie within the fine-grained deposits above (Figure 9C). Unlike muddy channel

bases, which typically have erosive surfaces to demark them (Hubbard *et al.*, 2014), confident identification of the exact top of the lobe within fine-grained deposits would be challenging. When no erosion is apparent, the deposits from the top of one lobe would likely transition into the base of the next with no recognizable change in sedimentary facies. Despite this, these findings prove useful in highlighting the bias of previous lobe deposit studies towards sandier intervals and call for a reassessment of where we interpret the tops and bases of hierarchical units within submarine fans (Spychala *et al.*, 2019).

5 | CONCLUSIONS

Using physical models with a signature of waxing-to-waning sediment supply, the interplay of external signals with internal processes within submarine fans has been evaluated. On the channelized slope, increasing sediment supply rate resulted in increased channel erosion and overbank deposition. The evolved channel dimensions improved flow efficiency, enhancing the external signal on the slope. Concurrently on the basin floor, the increasing rate of sediment supply led to forward-stepping of lobe elements, however, this was partially obscured by internal reorganization through compensational deposit stacking. When sediment supply rate was subsequently reduced, basin floor deposits back-stepped abruptly due to depositional relief to onlap the slope and infill the slope channel. Flows were then underfit with respect to the evolved channel dimensions and confined within the widened and deepened channel. Consequently, limited overbank deposition took place in the waning phase of sediment supply. This complex overall evolution resulted in deposits that were distinctly different in the waxing and waning phases of sediment supply, despite similar external input conditions.

A comparison of the slope and basin floor environments revealed that external factors have a stronger influence upon slope channels whilst internal processes dominate basin floor lobe deposits. These findings validate many conceptual models of submarine fans, including sediment supply driven progressive channel confinement, and how internal reorganization can shred external signals in the deepest parts of the sedimentary sink. Despite this internal 'dilution' of the external signal and the poorer preservation potential of deposits in the slope channel axis, the external signal could still be observed on the basin floor, with deposits from higher sediment supply rates extending farther into the basin before depositional relief dominated.

The recorded evolution of forward-stepping and compensation followed by abrupt back-stepping represents the signature of an entangled external-internal cycle of sedimentation in a submarine fan. This evolution is a possible

new mechanism to explain common vertical stacking patterns of coarsening and thickening upwards sandstone successions followed abruptly by thin-bedded fine-grained sediment in outcrop and core. These findings should encourage continued analysis of submarine fan architecture from a perspective that integrates both external and internal controlling mechanisms and provide a new evolutionary model to search for in natural systems. Future work may aim to test a range of different external signals such as variable sediment concentration or grain size to assess whether these have a different impact on the organization of submarine fans.

ACKNOWLEDGEMENTS

Equinor ASA is acknowledged for funding this research. Thony van der Gon Netscher is thanked for technical assistance with the experiments. Michael Clare and an anonymous reviewer are thanked for their insightful comments that broadened the scope of this work. Zane Jobe, Brian Romans, Peter Burgess, and an anonymous reviewer are thanked for their helpful comments on an earlier version of this manuscript. Chief Editor Peter Swart is thanked for handling the manuscript and Euan Soutter is acknowledged for digitizing Figure S9.

CONFLICT OF INTEREST

The authors have no conflict of interest to declare.

DATA AVAILABILITY STATEMENT

The data that support the findings of this study are available as supporting information. Any additional data requests can be made to the corresponding author.

ORCID

Ross A. Ferguson  <https://orcid.org/0000-0001-8089-825X>

Joris T. Eggenhuisen  <https://orcid.org/0000-0002-7389-9665>

REFERENCES

- Allin, J.R., Hunt, J.E., Clare, M.A. and Talling, P.J. (2018) Eustatic sea-level controls on the flushing of a shelf-incising submarine canyon. *GSA Bulletin*, 130, 222–237. <https://doi.org/10.1130/B31658.1>
- Azpiroz-Zabala, M., Cartigny, M.J.B., Talling, P.J., Parsons, D.R., Sumner, E.J., Clare, M.A. *et al.* (2017) Newly recognized turbidity current structure can explain prolonged flushing of submarine canyons. *Science Advances*, 3, 1–12. <https://doi.org/10.1126/sciadv.1700200>
- Beerbower, J.R. (1964) Cyclothems and cyclic depositional mechanisms in alluvial plain sedimentation. *Kansas State Geological Survey Bulletin*, 169, 31–42.
- Bernhardt, A., Jobe, Z.R. and Lowe, D.R. (2011) Stratigraphic evolution of a submarine channel-lobe complex system in a narrow fairway within the Magallanes foreland basin, Cerro Toro Formation, southern Chile. *Marine and Petroleum Geology*, 28, 785–806. <https://doi.org/10.1016/j.marpetgeo.2010.05.013>
- Bernhardt, A., Melnick, D., Hebbeln, D., Lückge, A. and Strecker, M.R. (2015) Turbidite paleoseismology along the active continental margin of Chile—Feasible or not? *Quaternary Science Reviews*, 120, 71–92. <https://doi.org/10.1016/j.quascirev.2015.04.001>
- Blum, M., Rogers, K., Gleason, J., Najman, Yani, Cruz, J. and Fox, L. (2018) Allogenic and autogenic signals in the stratigraphic record of the deep-sea Bengal Fan. *Scientific Reports*, 8, 7973. <https://doi.org/10.1038/s41598-018-25819-5>
- Boulestex, K., Poyatos-Moré, M., Flint, S.S., Taylor, K.G., Hodgson, D.M. and Hasiotis, S.T. (2019) Transport and deposition of mud in deep-water environments: Processes and stratigraphic implications. *Sedimentology*, 66(7), 2894–2925. <https://doi.org/10.1111/sed.12614>
- Burgess, P.M., Masiero, I., Toby, S.C. and Duller, R.A. (2019) A big fan of signals? Exploring autogenic and allogenic process and product in a numerical stratigraphic forward model of submarine-fan development. *Journal of Sedimentary Research*, 89, 1–12. <https://doi.org/10.2110/jsr.2019.3>
- Cantelli, A., Pirmez, C., Johnson, S. and Parker, G. (2011) Morphodynamic and stratigraphic evolution of self-channelized subaqueous fans emplaced by turbidity currents. *Journal of Sedimentary Research*, 81, 233–247. <https://doi.org/10.2110/jsr.2011.20>
- Cecil, C.B. (2003). The concept of autocyclic and allocyclic controls on sedimentation and stratigraphy, emphasising the climatic variable. In Cecil, C.B. and Edgar, N.T. (Eds.) *Climate Controls on Stratigraphy. SEPM Special Publications*, 77, 13–20. doi:<https://doi.org/10.2110/pec.03.77.0013>
- Clare, M.A., Talling, P.J., Challenor, P., Malgesini, G. and Hunt, J. (2014) Distal turbidites reveal a common distribution for large (> 0.1 km³) submarine landslide recurrence. *Geology*, 42, 262–266. <https://doi.org/10.1130/G35160.1>
- Covault, J.A., Romans, B.W., Fildani, A., McGann, M. and Graham, S.A. (2010) Rapid climatic signal propagation from source to sink in a Southern California sediment-routing system. *The Journal of Geology*, 118, 247–259. <https://doi.org/10.1086/651539>
- Covault, J.A., Romans, B.W., Graham, S.A., Fildani, A. and Hilley, G.E. (2011) Terrestrial source to deep-sea sink sediment budgets at high and low sea levels: insights from tectonically active Southern California. *Geology*, 39, 619–622. <https://doi.org/10.1130/G31801.1>
- Deptuck, M.E., Sylvester, Z., Pirmez, C. and O’Byrne, C. (2007) Migration–aggradation history and 3-D seismic geomorphology of submarine channels in the Pleistocene Benin–major Canyon, western Niger Delta slope. *Marine and Petroleum Geology*, 23, 406–433. <https://doi.org/10.1016/j.marpetgeo.2007.01.005>
- Deptuck, M.E., Piper, D.J.W., Savoye, B. and Gervais, A. (2008) Dimensions and architecture of late Pleistocene submarine lobes off the northern margin of East Corsica. *Sedimentology*, 55, 869–898. <https://doi.org/10.1111/j.1365-3091.2007.00926.x>
- Dorrell, R.M., Burns, A.D. and McCaffrey, W.D. (2015) The inherent instability of leveed seafloor channels. *Geophysical Research Letters*, 42(10), 4023–4031. <https://doi.org/10.1002/2015GL063809>
- Eggenhuisen, J.T., Tilston, M.C., de Leeuw, J., Pohl, F. and Cartigny, M.J.B. (2019) Turbulent diffusion modelling of sediment in turbidity currents: An experimental validation of the Rouse approach. *The Depositional Record*, 6, 1–14. <https://doi.org/10.1002/dep2.86>
- Emmel, F.J. and Curray, J.R. (1983) The Bengal submarine fan, north-eastern Indian Ocean. *Geo-Marine Letters*, 3, 119–124. <https://doi.org/10.1007/BF02462456>

- Fernandez, R.L., Cantelli, A., Pirmez, C., Sequeiros, O. and Parker, G. (2014) Growth patterns of subaqueous depositional channel lobe systems developed over a basement with a downdip break in slope: laboratory experiments. *Journal of Sedimentary Research*, 84, 168–182. <https://doi.org/10.2110/jsr.2014.10>
- Foreman, B.Z. and Straub, K.M. (2017) Autogenic geomorphic processes determine the resolution and fidelity of terrestrial paleoclimate records. *Science advances*, 3, e1700683. <https://doi.org/10.1126/sciadv.1700683>
- Grecula, M., Flint, S.S., Wickens, H.D.V. and Johnson, S.D. (2003) Upward-thickening patterns and lateral continuity of Permian sand-rich turbidite channel fills, Laingsburg Karoo, South Africa. *Sedimentology*, 50, 831–853. <https://doi.org/10.1046/j.1365-3091.2003.00576.x>
- Groenenberg, R.M., Hodgson, D.M., Pr el at, A., Luthi, S.M. and Flint, S.S. (2010) Flow-deposit interaction in submarine lobes: Insights from outcrop observations and realizations of a process-based numerical model. *Journal of Sedimentary Research*, 80, 252–267. <https://doi.org/10.2110/jsr.2010.028>
- Grundv ag, S.A., Johannessen, E.P., Helland-Hansen, W. and Plink-Bj orklund, P. (2014) Depositional architecture and evolution of progradationally stacked lobe complexes in the Eocene Central Basin of Spitsbergen. *Sedimentology*, 61, 535–569. <https://doi.org/10.1111/sed.12067>
- Gwiazda, R., Paull, C.K., Ussler, W. and Alexander, C.R. (2015) Evidence of modern fine-grained sediment accumulation in the Monterey Fan from measurements of the pesticide DDT and its metabolites. *Marine Geology*, 363, 125–133. <https://doi.org/10.1016/j.margeo.2015.02.006>
- de Haas, T., van den Berg, W., Braat, L. and Kleinhans, M.G. (2016) Autogenic avulsion, channelization and backfilling dynamics of debris-flow fans. *Sedimentology*, 63(6), 1596–1619.
- de Leeuw, J., Eggenhuisen, J.T. and Cartigny, M.J.B. (2016) Morphodynamics of submarine channel inception revealed by new experimental approach. *Nature Communications*, 7, 10886. <https://doi.org/10.1038/ncomms10886>
- de Leeuw, J., Eggenhuisen, J.T. and Cartigny, M.J.B. (2018a) Linking submarine channel–levee facies and architecture to flow structure of turbidity currents: insights from flume tank experiments. *Sedimentology*, 65, 931–951. <https://doi.org/10.1111/sed.12411>
- de Leeuw, J., Eggenhuisen, J.T., Spychala, Y.T., Heijnen, M.S., Pohl, F. and Cartigny, M.J.B. (2018b) Sediment volume and grain-size partitioning between submarine channel–levee systems and lobes: an experimental study. *Journal of Sedimentary Research*, 88, 777–794. <https://doi.org/10.2110/jsr.2018.46>
- Hamilton, P.B., Strom, K. and Hoyal, D.C. (2013) Autogenic incision-backfilling cycles and lobe formation during the growth of alluvial fans with supercritical distributaries. *Sedimentology*, 60(6), 1498–1525. <https://doi.org/10.1111/sed.12046>
- Harris, A.D., Covault, J.A., Madof, A.S., Sun, T., Sylvester, Z. and Granjeon, D. (2016) Three-dimensional numerical modeling of eustatic control on continental-margin sand distribution. *Journal of Sedimentary Research*, 86, 1434–1443. <https://doi.org/10.2110/jsr.2016.85>
- Harris, A.D., Baumgardner, S.E., Sun, T. and Granjeon, D. (2018) A poor relationship between sea level and deep-water sand delivery. *Sedimentary Geology*, 370, 42–51. <https://doi.org/10.1016/j.sedgeo.2018.04.002>
- Hodgson, D.M., Flint, S.S., Hodgetts, D., Drinkwater, N.J., Johannessen, E.P. and Luthi, S.M. (2006) Stratigraphic evolution of fine-grained submarine fan systems, Tanqua Depocenter, Karoo Basin, South Africa. *Journal of Sedimentary Research*, 76, 20–40. <https://doi.org/10.2110/jsr.2006.03>
- Hodgson, D.M., Kane, I.A., Flint, S.S., Brunt, R.L. and Ortiz-Karpf, A. (2016) Time-transgressive confinement on the slope and the progradation of basin-floor fans: implications for the sequence stratigraphy of deep-water deposits. *Journal of Sedimentary Research*, 86, 73–86. <https://doi.org/10.2110/jsr.2016.3>
- Hoyal, D.C.J.D. and Sheets, B.A. (2009) Morphodynamic evolution of experimental cohesive deltas. *Journal of Geophysical Research: Earth Surface*, 114, F02. <https://doi.org/10.1029/2007JF000882>
- Hubbard, S.M., Covault, J.A., Fildani, A. and Romans, B.W. (2014) Sediment transfer and deposition in slope channels: deciphering the record of enigmatic deep-sea processes from outcrop. *GSA Bulletin*, 126, 857–871. <https://doi.org/10.1130/B30996.1>
- Janocko, M., Cartigny, M.B.J., Nemecek, W. and Hansen, E.W.M. (2013a) Turbidity current hydraulics and sediment deposition in erodible sinuous channels: laboratory experiments and numerical simulations. *Marine and Petroleum Geology*, 41, 222–249. <https://doi.org/10.1016/j.marpetgeo.2012.08.012>
- Janocko, M., Nemecek, W., Henriksen, S. and Warchol, M. (2013b) The diversity of deep-water sinuous channel belts and slope valley-fill complexes. *Marine and Petroleum Geology*, 41, 7–34. <https://doi.org/10.1016/j.marpetgeo.2012.06.012>
- Jerolmack, D.J. and Paola, C. (2010) Shredding of environmental signals by sediment transport. *Geophysical Research Letters*, 37, L19401. <https://doi.org/10.1029/2010GL044638>
- Jobe, Z.R., Lowe, D.R. and Uchytel, S.J. (2011) Two fundamentally different types of submarine canyons along the continental margin of Equatorial Guinea. *Marine and Petroleum Geology*, 28, 843–860. <https://doi.org/10.1016/j.marpetgeo.2010.07.012>
- Jobe, Z.R., Sylvester, Z., Parker, A.O., Howes, N.C., Slowey, N. and Pirmez, C. (2015) Rapid adjustment of submarine channel architecture to changes in sediment supply. *Journal of Sedimentary Research*, 85, 729–753. <https://doi.org/10.2110/jsr.2015.30>
- Jobe, Z.R., Sylvester, Z., Howes, N., Pirmez, C., Parker, A., Cantelli, A. et al. (2017) High-resolution, millennial-scale patterns of bed compensation on a sand-rich intraslope submarine fan, western Niger Delta slope. *GSA Bulletin*, 129, 23–37. <https://doi.org/10.1130/B31440.1>
- Jobe, Z.R., Howes, N., Romans, B.W. and Covault, J.A. (2018) Volume and recurrence of submarine-fan-building turbidity currents. *The Depositional Record*, 4, 160–176. <https://doi.org/10.1002/dep2.42>
- Johnson, S.D., Flint, S.S., Hinds, D. and De Ville Wickens, H. (2001) Anatomy of basin floor to slope turbidite systems, Tanqua Karoo, South Africa. *Sedimentology*, 48, 987–1023. <https://doi.org/10.1046/j.1365-3091.2001.00405.x>
- Kane, I.A. and Hodgson, D.M. (2011) Sedimentological criteria to differentiate submarine channel levee subenvironments: exhumed examples from the Rosario Fm. (Upper Cretaceous) of Baja California, Mexico, and the Fort Brown Fm. (Permian), Karoo Basin, S. Africa. *Marine and Petroleum Geology*, 28, 807–823. <https://doi.org/10.1016/j.marpetgeo.2010.05.009>
- Kane, I.A., McCaffrey, W.D. and Peakall, J. (2008) Controls on sinuosity evolution within submarine channels. *Geology*, 36, 287–290. <https://doi.org/10.1130/G24588A.1>
- Kane, I.A. and Pont en, A.S.M. (2012) Submarine transitional flow deposits in the Paleogene Gulf of Mexico. *Geology*, 40, 1119–1122. <https://doi.org/10.1130/G33410.1>
- Kane, I.A., Kneller, B.C., Dykstra, M., Kassem, A. and McCaffrey, W.D. (2007) Anatomy of a submarine channel-lee: An example

- from Upper Cretaceous slope sediments, Rosario Formation, Baja California, Mexico. *Marine and Petroleum Geology*, 24, 540–563. <https://doi.org/10.1016/j.marpetgeo.2007.01.003>
- Kane, I.A., Pontén, A.S.M., Vangdal, B., Eggenhuisen, J.T., Hodgson, D.M. and Spychala, Y.T. (2017) The stratigraphic record and processes of turbidity current transformation across deep-marine lobes. *Sedimentology*, 64, 1236–1273. <https://doi.org/10.1111/sed.12346>
- Karamitopoulos, P., Weltje, G.J. and Dalman, R.A.F. (2014) Allogenic controls on autogenic variability in fluvio-deltaic systems: inferences from analysis of synthetic stratigraphy. *Basin Research*, 26, 767–779. <https://doi.org/10.1111/bre.12065>
- King, R.C., Hodgson, D.M., Flint, S.S., van Graham, J.P. and Lente, B. (2009) Development of subaqueous fold belts as a control on the timing and distribution of deepwater sedimentation: An example from the southwest Karoo Basin, South Africa. In Kneller, B., Martinsen, O.J. and McCaffrey, B. (Eds.) *External Controls on Deep-Water Depositional Systems. SEPM Special Publications*, 92, 261–278. doi: <https://doi.org/10.2110/sepm.092.261>
- Kneller, B. (2003) The influence of flow parameters on turbidite slope channel architecture. *Marine and Petroleum Geology*, 20, 901–910. <https://doi.org/10.1016/j.marpetgeo.2003.03.001>
- Kneller, B. and McCaffrey, W. (1999) Depositional effects of flow non-uniformity and stratification within turbidity currents approaching a bounding slope: deflection, reflection, and facies variation. *Journal of Sedimentary Research*, 69, 980–991. <https://doi.org/10.2110/jsr.69.980>
- Kneller, B., Bozetti, G., Callow, R., Dykstra, M., Hansen, L., Kane, I. et al. (2020). Architecture, process, and environmental diversity in a Late Cretaceous slope channel system. *Journal of Sedimentary Research*, 90, 1–26. <https://doi.org/10.2110/jsr.2020.1>
- Knudson, K.P. and Hendy, I.L. (2009) Climatic influences on sediment deposition and turbidite frequency in the Nitinat Fan, British Columbia. *Marine Geology*, 262, 29–38. <https://doi.org/10.1016/j.margeo.2009.03.002>
- Li, Q., Yu, L. and Straub, K.M. (2016) Storage thresholds for relative sea-level signals in the stratigraphic record. *Geology*, 44(3), 179–182. <https://doi.org/10.1130/G37484.1>
- MacDonald, H.A., Peakall, J., Wignall, P.B. and Best, J. (2011) Sedimentation in deep-sea lobe-elements: implications for the origin of thickening-upward sequences. *Journal of the Geological Society, London*, 168, 319–331. <https://doi.org/10.1144/0016-76492010-036>
- Maslin, M., Knutz, P.C. and Ramsay, T. (2006) Millennial-scale sea-level control on avulsion events on the Amazon Fan. *Quaternary Science Reviews*, 25(23–24), 3338–3345. <https://doi.org/10.1016/j.quascirev.2006.10.012>
- Middleton, G.V. and Southard, J.B. (1984) Mechanics of sediment movement. SEPM, Eastern Section Short Course 3 Providence, 401 pp. <https://doi.org/10.2110/scn.84.03>
- Mikeš, D., ten Veen, J.H., Postma, G. and Steel, R. (2015) Inferring autogenically induced depositional discontinuities from observations on experimental deltaic shoreline trajectories. *Terra Nova*, 27, 442–448. <https://doi.org/10.1111/ter.12178>
- Mohrig, D. and Buttles, J. (2007) Deep turbidity currents in shallow channels. *Geology*, 35, 155–158. <https://doi.org/10.1130/G22716A.1>
- Nelson, C.H., Escutia, C., Goldfinger, C., Karabanov, E., Gutierrez-Pastor, J. and De Batist, M. (2009) External controls on modern clastic turbidite systems: three case studies. In Kneller, B., Martinsen, O.J. and McCaffrey, B. (Eds.) *External Controls on Deep-Water Depositional Systems. SEPM Special Publications*, 92, 57–76. doi: <https://doi.org/10.2110/sepm.092.057>
- Normark, W.R. (1970) Growth patterns of deep-sea fans. *AAPG Bulletin*, 54, 2170–2195. <https://doi.org/10.1306/5D25CC79-16C1-11D7-8645000102C1865D>
- Normark, W.R., Piper, D.J.W. and Sliter, R. (2006) Sea-level and tectonic control of middle to late Pleistocene turbidite systems in Santa Monica Basin, offshore California. *Sedimentology*, 54, 867–897. <https://doi.org/10.1111/j.1365-3091.2006.00797.x>
- Pickering, K.T. (1983) Transitional submarine fan deposits from the late Precambrian Kongsfjord Formation submarine fan, NE Finnmark, N. Norway. *Sedimentology*, 30, 181–199. <https://doi.org/10.1111/j.1365-3091.1983.tb00664.x>
- Picot, M., Droz, L., Marsset, T., Dennielou, B. and Bez, M. (2016) Controls on turbidite sedimentation: insights from a quantitative approach of submarine channel and lobe architecture (Late Quaternary Congo Fan). *Marine and Petroleum Geology*, 72, 423–446. <https://doi.org/10.1016/j.marpetgeo.2016.02.004>
- Picot, M., Marsset, T., Droz, L., Dennielou, B., Baudin, F., Hermoso, M. et al. (2019) Monsoon control on channel avulsions in the Late Quaternary Congo Fan. *Quaternary Science Reviews*, 204, 149–171. <https://doi.org/10.1016/j.quascirev.2018.11.033>
- Pirmez, C. and Imran, J. (2003) Reconstruction of turbidity currents in Amazon Channel. *Marine and Petroleum Geology*, 20, 823–849. <https://doi.org/10.1016/j.marpetgeo.2003.03.005>
- Pohl, F., Eggenhuisen, J.T., Tilston, M. and Cartigny, M.J.B. (2019) New flow relaxation mechanism explains scour fields at the end of submarine channels. *Nature Communications*, 10, 4425. <https://doi.org/10.1038/s41467-019-12389-x>
- Posamentier, H.W. and Kolla, V. (2003) Seismic geomorphology and stratigraphy of depositional elements in deep-water settings. *Journal of Sedimentary Research*, 73, 367–388. <https://doi.org/10.1306/111302730367>
- Prather, B.E., Pirmez, C. and Winker, C.D. (2012). Stratigraphy of linked intraslope basins: Brazos-Trinity system, western Gulf of Mexico. In Prather, B.E., Deptuck, M.E., Mohrig, D.C., van Hoorn, B. and Wynn, R.B. (Eds.) *Application of the Principles of Seismic Geomorphology to Continental-Slope and Base-of-Slope Systems: Case Studies from Seafloor and Near-Seafloor Analogues. SEPM Special Publications*, 99, 83–109. <https://doi.org/10.2204/2010.1016/j.quascirev.2006.10.012>
- Prélat, A., Hodgson, D.M. and Flint, S.S. (2009) Evolution, architecture and hierarchy of distributary deep-water deposits: a high-resolution outcrop investigation from the Permian Karoo Basin, South Africa. *Sedimentology*, 56, 2132–2154. <https://doi.org/10.1111/j.1365-3091.2009.01073.x>
- Prélat, A., Covault, J.A., Hodgson, D.M., Fildani, A. and Flint, S.S. (2010) Intrinsic controls on the range of volumes, morphologies, and dimensions of submarine lobes. *Sedimentary Geology*, 232, 66–76. <https://doi.org/10.1016/j.sedgeo.2010.09.010>
- Rabouille, C., Dennielou, B., Baudin, F., Raimonet, M., Droz, L., Khripounoff, A. et al. (2019) Carbon and silica megasink in deep-sea sediments of the Congo terminal lobes. *Quaternary Science Reviews*, 222, 105854. <https://doi.org/10.1016/j.quascirev.2019.07.036>
- van Rijn, L.C. (1993) *Principles of Sediment Transport in Rivers, Estuaries and Coastal Seas*. Amsterdam, the Netherlands: Aqua Publications.
- Romans, B.W., Normark, W.R., McGann, M.M., Covault, J.A. and Graham, S.A. (2009) Coarse-grained sediment delivery and distribution in the Holocene Santa Monica Basin, California: implications

- for evaluating source-to-sink flux at millennial time scales. *GSA Bulletin*, 121, 1394–1408. <https://doi.org/10.1130/B26393.1>
- Romans, B.W., Castellort, S., Covault, J.A., Fildani, A. and Walsh, J.P. (2016) Environmental signal propagation in sedimentary systems across time-scales. *Earth-Science Reviews*, 153, 7–29. <https://doi.org/10.1016/j.earscirev.2015.07.012>
- Rouse, H. (1939) Experiments on the mechanics of sediment suspension. In *Proceedings of the 5th International Congress for Applied Mechanics*. New York: John Wiley, pp. 550–554.
- Shields, A. (1936) Anwendung der Aehnlichkeitsmechanik und der Turbulenzforschung auf die Geschiebebewegung. Preussischen Versuchsanstalt für Wasserbau.
- Shumaker, L.E., Jobe, Z.R., Johnstone, S.A., Pettinga, L.A., Cai, D. and Moody, J.D. (2018) Controls on submarine channel-modifying processes identified through morphometric scaling relationships. *Geosphere*, 14, 1–17. <https://doi.org/10.1130/GES01674.1>
- Sømme, T.O., Helland-Hansen, W., Martinsen, O.J. and Thurmond, J.B. (2009) Relationship between morphological and sedimentological parameters in source-to-sink systems: a basis for predicting semi-quantitative characteristics in subsurface systems. *Basin Research*, 21, 361–387. <https://doi.org/10.1111/j.1365-2117.2009.00397.x>
- Spychala, Y.T., Hodgson, D.M., Prélat, A., Kane, I.A., Flint, S.S. and Mountney, N.P. (2017) Frontal and lateral submarine lobe fringes: Comparing sedimentary facies, architecture and flow processes. *Journal of Sedimentary Research*, 87, 75–95. <https://doi.org/10.2110/jsr.2017.2>
- Spychala, Y.T., Eggenhuisen, J.T., Tilston, M. and Pohl, F. (2019) The influence of basin settings and flow properties on the dimensions of submarine lobe elements. Preprint at <https://eartharxiv.org/sk8v3/>
- Straub, K.M. and Pyles, D.R. (2012) Quantifying the hierarchical organization of compensation in submarine fans using surface statistics. *Journal of Sedimentary Research*, 82, 889–898. <https://doi.org/10.2110/jsr.2012.73>
- Straub, K.M., Paola, C., Mohrig, D., Wolinsky, M.A. and George, T. (2009) Compensational stacking of channelized sedimentary deposits. *Journal of Sedimentary Research*, 79, 673–688. <https://doi.org/10.2110/jsr.2009.070>
- Talling, P.J., Wynn, R.B., Masson, D.G., Frenz, M., Cronin, B.T., Schiebel, R. et al. (2007) Onset of submarine debris flow deposition far from original giant landslide. *Nature*, 450, 541–544. <https://doi.org/10.1038/nature06313>
- Toby, S.C., Duller, R.A., De Angelis, S. and Straub, K.M. (2019) A stratigraphic framework for the preservation and shredding of environmental signals. *Geophysical Research Letters*, 46(11), 5837–5845. <https://doi.org/10.1029/2019GL082555>
- Wang, Y., Straub, K.M. and Hajek, E.A. (2011) Scale-dependent compensational stacking: An estimate of autogenic time scales in channelized sedimentary deposits. *Geology*, 39, 811–814. <https://doi.org/10.1130/G32068.1>
- Xu, J.P., Sequeiros, O.E. and Noble, M.A. (2014) Sediment concentrations, flow conditions, and downstream evolution of two turbidity currents, Monterey Canyon, USA. *Deep Sea Research Part I: Oceanographic Research Papers*, 89, 11–34. <https://doi.org/10.1016/j.dsr.2014.04.001>
- Yang, W., Kominz, M.A. and Major, R.P. (1998) Distinguishing the roles of autogenic versus allogenic processes in cyclic sedimentation, Cisco Group (Virgilian and Wolfcampian) north-central Texas. *GSA Bulletin*, 110, 1333–1353. [https://doi.org/10.1130/0016-7606\(1998\)110%3C1333:DTROAV%3E2.3.CO;2](https://doi.org/10.1130/0016-7606(1998)110%3C1333:DTROAV%3E2.3.CO;2)

SUPPORTING INFORMATION

Additional supporting information may be found online in the Supporting Information section.

How to cite this article: Ferguson RA, Kane IA, Eggenhuisen JT, et al. Entangled external and internal controls on submarine fan evolution: an experimental perspective. *Depositional Rec.* 2020;6:605–624. <https://doi.org/10.1002/dep2.109>